Subsurface warming in the tropical Atlantic for the last 3 deglaciations: Insights from organic molecular proxies

Rouyer-Denimal Louis [1, *], Govin Aline [2], Bouloubassi Ioanna [3], Nguyen Tu Thanh Thuy [1], Albuquerque Ana Luiza Spadano [4], Anquetil Christelle [1], Huguet Arnaud [1, *]

[1] Sorbonne Université/CNRS/EPHE, UMR 7619 METIS, Paris, France
[2] LSCE-IPSL Laboratoire des Sciences du Climat et de l'Environnement (CEA-CNRS-UVSQ), Université Paris Saclay, Gif-sur-Yvette, France
[3] Sorbonne Université/CNRS/IRD/MNHN, LOCEAN, Paris, France
[4] Universidade Federal Fluminense, Departamento de Geologia & Geofisica, Niterói, Rio de Janeiro, Brazil

* Corresponding authors : Louis Rouyer-Denimal, email address :
louis.rouyer-denimal@sorbonne-universite.fr ; Arnaud Huguet, email address :
arnaud.huguet@sorbonne-universite.fr

Abstract :

During glacial terminations, the role of cross-equatorial currents in the northward spreading of warm and salty waters is essential to the reach of the following interglacial state. In the western tropical Atlantic, where the interhemispheric North Brazil Current develops, most of the existing temperature records focused on the last deglaciation. Here, using a marine sediment core covering the last 305 kyr before present (BP), we present two records of the surface (mixed layer) and the subsurface (upper thermocline) temperatures based on organic proxies UK'37 and TEXH86, respectively. During the last three glacial terminations, these records exhibit large temperature increases especially in the subsurface layer. We suggest the combined influences of the thermal bipolar seesaw and the Agulhas Leakage, acting together to warm the interior South Atlantic, to explain the strong warming of the tropical western Atlantic thermocline (+5 °C) during these periods of reduced Atlantic meridional overturning circulation (AMOC). In addition, we propose an enhanced cross-equatorial gyre to elucidate the synchronous deglacial warming of the western and eastern sides of the tropical Atlantic. The resumption of the AMOC at the onset of the following interglacial leads to the release of heat stored in thermocline waters mainly in the whole South Atlantic, as highlighted by the sharp upper ocean cooling recorded at the end of the deglacial interval. The combination of this temperature record and previously published ones in the western tropical Atlantic confirms the strong sensitivity of the upper ocean to AMOC changes in this region.

Highlights

► $U^{K'}_{37}$-SST and TEX^{H}_{86}-SubT temperatures were reconstructed over the last 305 kyr BP. ► Large subsurface warmings were highlighted over the last three deglaciations. ► The thermal bipolar seesaw model explains part of the temperature increase. ► Agulhas Leakage waters also contributed to the warming. ► An intensified cross-equatorial gyre explains the deglacial spreading of warm waters.

Keywords : Quaternary, Deglaciation, Paleoceanography, South Atlantic, Upper Ocean Temperature, Marine biomarkers, UK' 37, TEXH 86, Cross-equatorial gyre

1. Introduction

The Atlantic meridional overturning circulation (AMOC) plays a key role in the Earth's climate system (Buckley and Marshall, 2016; Trenberth and Fasullo, 2017). The AMOC experienced strong changes at both millennial and orbital scales over the late Pleistocene (Kageyama et al., 2010; Menviel et al., 2020; Paillard, 1998). Changes in AMOC intensity affected the spatial distribution of heat and water budgets (e.g. Castañeda et al., 2009; Wang et al., 2004), the atmospheric concentration

2

of carbon dioxide (e.g. Deaney et al., 2017; Ma et al., 2021) and the intensity of monsoon regimes over the globe (e.g. Rodríguez-Zorro et al., 2020; Simon et al., 2015). Future projections suggest an AMOC slowdown in response to the anthropogenic climate change (Liu et al., 2020). Therefore, it appears crucial to fully understand AMOC behaviour and associated climatic changes to elucidate, among others, the future evolution of Earth's system.

40   In the course of the late Pleistocene, millennial-scale events of massive icebergs discharges in the North Atlantic (Heinrich, 1988) were responsible of substantial AMOC weakening (McManus et al., 2004). The melting of these large ice blocks leaded to considerable freshwater inputs to the North Atlantic surface waters reducing the North Atlantic Deep Water production (Lynch-Stieglitz, 2017). As a result, the AMOC weakening induces a decrease of northward heat advection and thus a warming (cooling) in the South (North) Atlantic. Attempts to explain this opposite climatic behaviour between the North and the South

45   Atlantic rely on the bipolar seesaw thermodynamic model (Broecker et al., 1990; Crowley, 1992; Stocker and Johnsen, 2003). These "Heinrich events" occurred during some of the cold phase of the Dansgaard-Oeschger cycles, i.e. Greenland stadials (Bond et al., 1992; Rasmussen et al., 2014; Stocker, 2000) and deglaciations (Denton et al., 2010; Knorr and Lohmann, 2007). Glacial terminations are also associated with a poleward shift of the southern subtropical front, leading to an increase in the Agulhas Leakage (Bard and Rickaby, 2009). Indeed, this sudden deglacial outflow of saline and warm waters originating from

50   the Indo-Pacific oceans and propagating over the South Atlantic through the Cape basin is proposed to play a key role in the triggering of interglacial periods (Caley et al., 2011; Durgadoo et al., 2013; Peeters et al., 2004). As a consequence, the South Atlantic turns into a large heat reservoir during deglacial periods and abrupt climatic changes, with major reorganizations of the Earth's climate system such as a southward migration of the intertropical convergence zone (ITCZ) over the tropical South Atlantic (McGee et al., 2014; Portilho-Ramos et al., 2017).

55   The western tropical Atlantic is the oceanic gateway between the North and the South Atlantic where the interhemispheric North Brazil Current (NBC) forms (Rodrigues et al., 2007). This region experienced strong changes in response to Heinrich events and associated decrease in AMOC intensity. The reduced cross-equatorial transport by the North Brazil Current (Vink et al., 2001) led to an accumulation of warm waters in the western tropical Atlantic, as generally exhibited by surface temperature records (Crivellari et al., 2019; Nace et al., 2014; Weldeab et al., 2006). However, some temperature proxies

60   disagree with such warming trend, probably due to non-thermal influences on theses proxies (e.g. Jaeschke et al., 2007). This

general warming of the tropical and South Atlantic then caused a southward migration of the ITCZ (Portilho-Ramos et al., 2017), a weakening of southeasterly (SE) trades (Kim and Schneider, 2003) and a shoaling of the thermocline (Venancio et al., 2018). Moreover, in freshwater hosing experiments, the modelled tropical surface and thermocline layers exhibit large temperature increases and circulation changes (Chang et al., 2008; Dahl et al., 2005; Laurian and Drijfhout, 2011).

65   Paleotemperature proxies based on lipid biomarkers, namely long-chain C_{37}-alkenones and isoprenoid glycerol dialkyl glycerol tetraethers (iGDGTs), are among the most largely used to reconstruct past upper ocean temperatures. The distribution of long-chain C_{37}-alkenones, produced by *Prymnesiophyceae* algae, has been related to seawater temperature in both culture (Prahl and Wakeham, 1987), marine particles (Conte et al., 2006) and sediment studies (Müller et al., 1998; Tierney and Tingley, 2018) through the $U^{K'}_{37}$ index. *Prymnesiophyceae* can thrive in different depths into the euphotic zone. In the

70   oligotrophic (nutrient-poor) South Atlantic waters, they mostly develop in the lower euphotic zone (Cordeiro et al., 2013), where they find both light and nutrients (the deep chlorophyll maximum, Latasa et al., 2017) supplied by underlying waters (Benthien and Müller, 2000; Gérikas Ribeiro et al., 2016; Latasa et al., 2017). In the western tropical Atlantic, alkenones producers have been reported to thrive mainly above the thermocline, between 50 and 100 m depth (Dauner et al., 2019; Poulton et al., 2017) into the mixed layer. The C_{37}-alkenones $U^{K'}_{37}$ index can be used as a temperature proxy of this layer (later

75   referred as surface, Figure 1).

    Isoprenoid glycerol dialkyl glycerol tetraethers (iGDGTs) are produced by marine *Thaumarchaeota*, and their distribution, reflected in the TEX_{86} index, is strongly correlated with seawater temperature (Kim et al., 2010; Schouten et al., 2002; Tierney and Tingley, 2014). These chemo-autotroph ammonia-oxidizers archaea may develop within the whole water column (Ceccopieri et al., 2018; Zhang and Liu, 2018) but are prominent below the euphotic zone (Hurley et al., 2018), close to the

80   NO_2^- maximum. Depending on local settings, this maximum is observed in the mixed layer (surface; Dauner et al., 2019) or below, in the upper thermocline (subsurface; Zakem et al., 2018). In oligotrophic and highly stratified waters like the western tropical Atlantic, *Thaumarchaeota* develop in the upper thermocline because of a shallow thermocline and competition with primary producers (Inglis and Tierney, 2020; Schouten et al., 2013; Smith et al., 2014). This implies that the TEX_{86} can be used as a proxy of the upper thermocline temperature (hereafter referred as subsurface, Figure 1). The complementarity of the

85    $U^{K'}_{37}$ and TEX_{86} temperature proxies was shown by previous studies carried out in the eastern tropical Atlantic (Lopes dos

Santos et al., 2010), in the subtropical South Atlantic (Dauner et al., 2019), in the South China Sea (Li et al., 2013) and in the gulf of California (McClymont et al., 2012).

The sediment cores investigated so far in the western tropical Atlantic cover at most the last 200 kyr BP, mainly focusing on the last glacial cycle (Behling et al., 2000; Dauner et al., 2019) and the last deglaciation (Chiessi et al., 2015; Meier et al., 2021; Santos et al., 2022). In this study, we reconstructed the variations of upper ocean temperature using a marine sediment core collected in the western tropical Atlantic and covering the last 305 kyr BP. The surface and subsurface temperature records presented here, which are based on the $U^{K'}_{37}$ and TEX^{H}_{86} organic proxies, respectively, cover, for the first time in this area, the last three glacial terminations, with a higher temporal resolution during interglacial and deglacial times. We aimed to examine the response of the upper ocean temperature (surface and subsurface) in conjunction with changes in ocean stratification and atmospheric reorganizations, especially during deglacial AMOC slowdowns. We investigated the role of both the bipolar seesaw and Agulhas Leakage outflow to explain the magnitude of the strong upper ocean warmings reconstructed during glacial terminations in the western tropical Atlantic.

2. Material and Methods

2.1 Regional oceanographic settings

South Atlantic surface waters originate from both Indian, Pacific and Southern Oceans (Mignac et al., 2018). The subtropical gyre is the main circulation feature in the South Atlantic (Figure 1). This anticyclonic gyre flows, on average at the surface, between ~10°S and ~20°S (NW boundary) and 40°S (southern boundary) (Schettini et al., 2017; Stramma and England, 1999). In the first 800 m depth, the South Atlantic Central Waters (SACW) are the dominant water mass and they are fed by exchanges with the Indian, Pacific and Southern Oceans. Southern Ocean waters enter the subtropical gyre through the Malvinas Current (~200 – 400 m depth, SW corner) to supply the South Atlantic Current (SAC) flowing eastward (Figure 1). Around the Cape Basin, the South Atlantic Current meets the Indo-Pacific waters spreading through the Agulhas Leakage (AL) rings and eddies (~100 – 600 m depth) (Souza et al., 2018). Agulhas waters are an important supply of heat and salt to the South Atlantic (Beal et al., 2011). These waters mix with the South Atlantic Current to form the South Equatorial Current (SEC) flowing across the South Atlantic in a northwestward direction (Figure 1). The southern branch of the South Equatorial

Current (sSEC) bifurcates at the northwestern boundary and forms the Brazil Current and the North Brazil Undercurrent (NBUC) flowing southward and northward respectively (Rodrigues et al., 2007). The NBUC is a subsurface current along the Northeast Brazil that mixes with the South Equatorial Current to form the North Brazil Current (NBC; Goes et al., 2005; Krelling et al., 2020; Schott et al., 1998). This North Brazil Current is the main surface interhemispheric pathway linking the South and North Atlantic basins.

The core studied here is located at the northernmost position of the bifurcation of the southern branch of the South Equatorial Current, around 10°S (Rodrigues et al., 2007). At this location, surface waters are predominantly tropical waters (high salinity and temperature) with minor contributions (3 – 5%) of fresh and relatively cold coastal waters of riverine origin (Schettini et al., 2017). Mean annual sea surface temperature (SST) and salinity (SSS) at the core site are 27.7°C and 36.3 psu respectively (Locarnini et al., 2013). The mixed layer is 70 – 90 m deep and overlies on a thermocline that extends up to 300 m (Figure 1). Seasonal variability of temperature and stratification of the upper layer is very low at this location. The temperature of the mixed layer oscillates between 26.3°C and 28.1°C and its width varies between 70 and 120 m, while the thermocline depth and temperature are overall constant over the year (80 – 120 m depth for the upper thermocline with an average temperature of 25°C).

2.2 Sediment core and age model

The marine sediment core GL-1180 (8°27'18"S, 33°32'53"W, 1 037 m water depth) was collected on the Northeastern Brazilian margin, in the western tropical Atlantic ocean by the Petrobras oil company as described by Nascimento et al. (2021b) and stored at low temperature (4°C). 135 depths were subsampled corresponding to a resolution of 1.5 kyr and 7.1 kyr for deglacial/interglacial times and glacial periods, respectively. After sampling, sediments were freeze-dried and then stored at room temperature prior to preparation for lipid biomarker analyses.

We use the published age model of GL-1180 core, which is detailed in Nascimento et al. (2021b). Briefly, 6 depths were selected for radiocarbon (^{14}C) dating on *Globigerinoides ruber* and *Trilobatus sacculifer* shells by AMS (Accelerator Mass Spectrometry). The age model is also based on the visual alignment between the benthic foraminifera (*Cibicidoides sp.*) δ^{18}O and the global reference stack LR04 (Lisiecki and Raymo, 2005). It was then constructed using Bacon software v2.3 (Blaauw and Christen, 2011). Records of stable oxygen (δ^{18}O) and carbon (δ^{13}C) isotopic composition measured on the thermocline

135 (*Globorotalia truncatulinoides*) and benthic (*Cibicides spp.*) foraminifera species are available along the GL-1180 core

(Nascimento et al., 2021a).

2.3 Sample preparation

For each sample of core GL-1180 taken for lipid biomarker analyses, between 5 and 10 g of dry sediment (corresponding

to 1 cm of sediment), were extracted using a mixture of dichloromethane/methanol (CH_2Cl_2/CH_3OH), 9/1 (v/v) in an ultrasonic

140 bath. The extraction consisted in five ultrasonication cycles (10 min each) followed by centrifugation (5 min $\times$ 3 000 rpm)

using 20 mL, 15 mL and 10 mL (for the three last cycles only) of solvent mixture. The supernatants were combined,

concentrated to dryness using rotary evaporator and dissolved into 8 mL of CH_2Cl_2/CH_3OH, 9/1 (v/v).

Separation of the total lipid extract into three fractions of increasing polarity was performed over activated (150°C, ≥ 2 h)

and extracted (CH_2Cl_2 followed by *n*-heptane) silica (0.8 g of SiO_2 per column). The first fraction (apolar fraction) was eluted

145 with 5.5 mL of *n*-heptane, the second fraction containing alkenones with 8 mL of a mixture of heptane/ethyl acetate, 92.5/7.5

(v/v) and finally the third fraction containing GDGT with 8 mL of CH_2Cl_2/CH_3OH, 1/1 (v/v). The fractions were concentrated

at 35°C to dryness under gentle N_2 flux and dissolved into 2 mL of solvent corresponding to the mixture used for the elution

of the respective fraction.

2.4 Lipid biomarker analyses

150 Alkenone analyses were performed using a gas chromatograph coupled with a flame ionization detector (GC-FID) HP

6890 Series plus and equipped with an autosampler. Separation was carried out using an Agilent CP-Sil 5 CB column (50 m

$\times$ 0.32 mm, 0.25 µm inner diameter film thickness). Injections were performed with 5-α-cholestane (4 ppm final concentration)

as injection standard in on-column mode. Helium was used as carrier gas at a constant flow of 2 mL/min. The GC oven program

was: 50 °C to 140 °C at 30 °C/min, then to 280 °C at 20 °C/min and finally to 305 °C at 0.5 °C/min. Individual alkenones were

155 identified based on their retention times. For 14 samples (0 – 45, 75 – 105, 135, 150, 560 and 660 cm), alkenones were below

the detection limit.

GDGTs were analysed by a high-pressure liquid chromatography coupled with mass spectrometry with an atmospheric

pressure chemical ionization source (HPLC–APCI-MS) using a Shimadzu LCMS 2020 in selected ion monitoring mode, with

a procedure slightly modified from Hopmans et al. (2016) and Huguet et al. (2019). Briefly, GDGT analysis was performed
using two Acquity UHPLC BEH HILIC columns in tandem (150 mm × 2.1 mm, 1.7 µm; Waters, USA), thermally controlled
at 40°C. Injection volume was 30 µL. The flow rate was set at 0.2 mL/min. GDGTs were eluted isocratically for 25 min with
82%A/18% B, followed by a linear gradient to 65%A/35% B in 25 min, then a linear gradient to 100% B in 30 min, and back
to 82%A/18% B in 4 min, maintained for 50 min (A= hexane, B=hexane/isopropanol 9/1, v/v). Semi-quantification of iGDGTs
and brGDGTs was performed by comparing the integrated signal of the respective compound with the signal of a C_{46}
synthesised internal standard (Huguet et al., 2006) assuming their response factors to be identical.

2.5 Lipid-based temperature proxies

2.5.1 Core tops used for the selection of temperature proxy calibrations

We used published lipid-based data on core tops (0–1 cm) close to the location of core GL-1180 (–8.5°S, –34°W) to
determine the most accurate calibration (i.e. exhibiting the lowest residual error) to convert the $U^{K'}_{37}$ and TEX_{86} values into
temperatures. $U^{K'}_{37}$ and TEX_{86} values from these core tops were obtained from dataset published in Benthien and Müller (2000)
and Kim et al. (2008), respectively. We tested different $U^{K'}_{37}$ and TEX_{86} calibrations and compared the calculated temperature
estimates to modern *in situ* sea temperatures values from the World Ocean Atlas 13 (WOA 13; Locarnini et al., 2013). We
used both mean annual and seasonal temperatures over the period 1955-2014 for the comparison. When needed, spatial
interpolation with DIVA gridding was performed using the Ocean Data View software (Schlitzer, 2020) to better fit with the
location of core top temperature data.

2.5.2 The $U^{K'}_{37}$ index as a mixed layer temperature proxy

Past sea surface (mixed layer) temperatures in core GL-1180 were reconstructed using the long-chain alkenones (C_{37} di-
or tri-unsaturated methyl-ketones) through calculation of the $U^{K'}_{37}$ index (Eq. 1; Prahl and Wakeham, 1987):

$$U^{K'}_{37} = \frac{[C_{37:2}]}{[C_{37:2}] + [C_{37:3}]} \ (eq.\,1)$$

where [C$_{37:x}$] refers to the fractional abundance of C$_{37}$ alkenone with x insaturations

8

The main environmental variable influencing the $U^{K'}_{37}$ index is seawater temperature (Prahl and Wakeham, 1987). Nevertheless, non-thermal factors (i.e. lateral transport, seasonality and nutrient availability) can impact the $U^{K'}_{37}$ signal and all these processes have to be constrained before application of the index as a temperature proxy. They were examined close to the GL-1180 location by Benthien and Müller (2000), who highlighted the main influence of seawater temperature on the $U^{K'}_{37}$ signal in the western tropical Atlantic.

Various global and regional calibrations were developed to convert the $U^{K'}_{37}$ values into sea surface temperature (SST) estimates (Conte et al., 2006; Tierney and Tingley, 2015 and references therein). Based on the core top data in our study area, we found that the global calibration (60°N-60°S, core top calibration, mean annual SST at 0 m depth, Müller et al., 1998; eq. 2) yields the most accurate reconstruction of modern SST (mean residual error of 0.3°C), even though all tested calibrations provided realistic values (residual errors < 1°C; see Supplementary Table S1 and Figure S2).

$$SST = \frac{\left(U^{K'}_{37} - 0.044\right)}{0.033} \quad (R^2 = 0.96, n = 370, Error: \pm 1°C)(eq.2)$$

In the oligotrophic waters of the western tropical Atlantic, alkenones producers thrive preferentially in the lower mixed layer (see 1. Introduction). As the main export of alkenones is reported within the mixed layer (Dauner et al., 2019), we assume that the $U^{K'}_{37}$ is a surface proxy reconstructing the temperature of this layer (surface, $U^{K'}_{37}$-SST), as generally observed in the study area (Crivellari et al., 2019; Müller and Fischer, 2004; Sikes et al., 1991). The calibration standard error (±1σ; Müller et al., 1998) and total analytical error were respectively of 1°C (0.03 $U^{K'}_{37}$ unit) and 0.31°C (0.01 $U^{K'}_{37}$ unit). The analytical error was evaluated on the replicated injection of 10 different samples.

2.5.3 The TEX_{86} index as an upper thermocline temperature proxy

Past temperature of the subsurface (upper thermocline) was reconstructed based on the TEX_{86} index, calculated as follows (Schouten et al., 2002):

$$TEX_{86} = \frac{[GDGT - 2] + [GDGT - 3] + [Cren']}{[GDGT - 1] + [GDGT - 2] + [GDGT - 3] + [Cren']} (eq.3)$$

where [GDGT-X] refers to the fractional abundance (relative to total iGDGTs) of compound GDGT-X and Cren' is the regio-isomer of crenarchaeol. See Figure 2 for respective molecular structures.

9

205   Other factors than temperature were reported to have an influence on the distribution of iGDGTs. Thus, even though the TEX$_{86}$ index is based on the distribution of iGDGTs produced by marine *Thaumarchaeota*, these lipids are synthesised by all archaea (Inglis and Tierney, 2020), notably terrestrial *Thaumarchaeota* (Hopmans et al., 2004), methanogenic (Inglis et al., 2015) and methanotrophic archaea (Zhang et al., 2011). In order to constrain the effect of non-marine *Thaumarchaeota*-derived iGDGTs on the TEX$_{86}$ signal, we calculated the diagnostic ratios previously developed (Weijers et al., 2014; Zhang et al.,

210   2016, 2011). The values obtained (Supplementary Figure S1, Table S2) confirmed that in our record, marine *Thaumarchaeota* are the main iGDGT producers and that seawater temperature is the main factor influencing the iGDGT distribution.

      Among all developed surface and subsurface calibrations based on the TEX$_{86}$ index, the calibration based on the logarithmic transformation of the TEX$_{86}$ i.e. TEX$^{H}_{86}$ was specifically designed for "warm environments" i.e. SST > 15°C (Kim et al., 2010) and the Bayesian calibration developed by (Tierney and Tingley, 2014) is the most up to date.

215   Using the same approach as for U$^{K'}_{37}$ temperature calibration selection, we selected the calibration based on the TEX$^{H}_{86}$ index (eq. 4; Kim et al., 2010) as this calibration provides the most accurate (residual error of -1.5°C on average; see Supplementary Table S3 and Figure S2) SST estimates for our study area.

$$TEX^{H}_{86} = log(TEX_{86}) \quad ; \quad SST = 68.4 * TEX^{H}_{86} + 38.6 \quad (R^2 = 0.87, n = 255, \text{Error:} \pm 2.5°C, \pm 1\sigma) \text{ (eq. 4)}$$

      Since in the south western tropical Atlantic the *Thaumarchaeota* preferentially develop below the mixed layer and within

220   the upper thermocline (see 1. Introduction) we use the TEX$^{H}_{86}$ as a subsurface i.e. upper thermocline temperature proxy (hereafter mentioned as TEX$^{H}_{86}$-SubT). The total analytical error is of 0.01 TEX$_{86}$ unit (0.8°C for TEX$^{H}_{86}$ temperature) based on duplicate injections of 3 different samples.

3. Results

      U$^{K'}_{37}$-derived sea surface temperatures varied between 26.1 and 28.9°C (Figure 3). They show a typical glacial-interglacial

225   pattern with high values (28.1°C on average) found during the 230 – 185 and 132 – 70 kyr BP intervals, corresponding to MIS 7 (penultimate interglacial) and MIS 5 (last interglacial), respectively. The sharp increase of SST before these intervals of high SST correspond to the deglacial periods of Terminations II and III (TII and TIII), beginning at 133 and 250 kyr BP,

10

respectively. Even though the record is not continuous over the last 30 kyr, the SST increased starting from around 20 kyr BP and remained high (~28.5°C) during the Holocene (Figure 3).

230   The TEX^H_{86} upper thermocline temperature values ranged between 23.5°C and 29.4°C (Figure 3). The upper thermocline temperature values reconstructed with TEX^H_{86} are generally lower (1.4°C on average) and show a larger range of variations than the $U^{K'}_{37}$-SST record. TEX^H_{86}-SubT also shows a glacial-interglacial pattern, with high temperature values during MIS 7, MIS 5 and the Holocene. However, deglaciation intervals exhibit the highest temperature increases in the whole TEX^H_{86}-SubT and $U^{K'}_{37}$-SST records.

235   During Termination III, $U^{K'}_{37}$-SST and TEX^H_{86}-SubT records increased to reach a maximum around 245 kyr BP and started to decrease at the end of the deglacial interval (Figure 3). A similar temperature evolution is observed in both $U^{K'}_{37}$-SST and TEX^H_{86}-SubT records but the upper thermocline temperature only decreases before the onset of the following interglacial. Termination I shows a decrease in the TEX^H_{86}-SubT record around 14 kyr BP corresponding to the Bølling-Allerød period, while the Younger Dryas and Heinrich Event 1 are associated with high TEX^H_{86}-SubT values (Figure 3) . Besides, $U^{K'}_{37}$-SST

240   and TEX^H_{86}-SubT increased at the onset of Termination II and remained high over the whole interval. The temperature decrease of the TEX^H_{86}-SubT record preceded the one of $U^{K'}_{37}$-SST by approximately three thousand years.

        Furthermore, the TEX^H_{86}-SubT (but not the $U^{K'}_{37}$-SST) record exhibited strong increases during the transitions between the substages of the MIS 7 (MIS7a-7b and MIS 7c-7d). This temperature pattern was not observed during the MIS 5 and is specific to MIS 7 (Figure 3). Finally, at the onset of interglacial conditions, the TEX^H_{86}-SubT records starts to decrease which contrasts to the relatively stable $U^{K'}_{37}$-SST evolution (for TI and TII) during optimum interglacial periods. This feature is

245   particularly visible during the Last Interglacial (Figure 3).

4. Discussion

4.1 Upper Ocean warmings during glacial terminations of the last 305 kyr on the western boundary of the South Atlantic

250   Based on the GL-1180 core, the western tropical Atlantic experienced a warming in its upper limb over the last three glacial terminations (Figures 3 and 4). The warming of the ocean upper limb is a well described feature for the last two terminations as reported by previous studies along the Brazilian margin (Figure 4). During Termination 1, the upper thermocline experienced

temperature increase (Heinrich Event 1, H1, Younger Dryas, YD) and decrease (Bølling-Allerød, B/A) related to changes in upper layer heat transport. The H1 and YD events are associated with strong AMOC reduction (Lynch-Stieglitz, 2017) leading to a decrease in the cross-equatorial heat transport (Laurian and Drijfhout, 2011) and warm water accumulation in the South Atlantic (Arz et al., 1999; Chiessi et al., 2008; Santos et al., 2017). The deglacial seawater warming is common to the whole western South Atlantic, as exhibited by a stack of 17 surface temperature records (Santos et al., 2022, Figure 4C) from the Brazilian margins. However, in our records (Figure 3), the amplitude of the warming is lower in surface (+1.5°C) compared to upper thermocline (+4°C) waters, indicating warm water accumulation at deeper levels, as observed in freshwater hosing experiments (e.g. Rühlemann et al., 2004).

Over Termination II, the GL-1180 temperature records present similarities with those of the GL-1090 core (Brazilian margin, ~25°S) (see Figure 1 for core locations) in respect to: (i) the occurrence of temperature increase, (ii) the larger amplitude of the warming at the subsurface (upper and main thermocline) compared to the surface and (iii) the surface and subsurface decrease at the onset of the last interglacial (Figure 4A, B). In the GL-1090 temperature records, the vertical temperature gradient is stronger for organic proxies ($U^{K'}_{37}$ and TEX^H_{86}) than for foraminifera-based (*G. ruber*, *G. inflata*) Mg/Ca records. At this location, these differences can be explained by distinct habitat depths between *G. ruber* and the Thaumarchaeota (mixed layer), the haptophytes (upper thermocline) and *G. inflata* (main thermocline). The habitat depth is actually controlled by nutrient and lights supplies, themselves constrained by the structure of the water column (Hurley et al., 2018; Latasa et al., 2017). Such differences between organic and inorganic proxies have already been highlighted and attributed to distinct habitat depths, seasonality and transport to the sediment (Dauner et al., 2019; Richey et al., 2011). In addition, temporal changes in the structure of the upper water column could also lead to diverging temperature estimates from organisms dwelling at distinct depths.

In contrast, the GL-1180 temperature record of the main thermocline (*G. truncatulinoides)* differs clearly from the surface and upper thermocline records (Figure 3). First, the temperature estimates based on the TEX^H_{86} index are higher than those based on the Mg/Ca ratio (*G. truncatulinoides)*. This is in agreement with a shallower signal recorded by Thaumarchaeota (upper thermocline) compared to *G. truncatulinoides* (main thermocline). Secondly, there is no deglacial warming indicated by the main thermocline temperature record. In contrast, a precessional pace have been identified in the stratification proxy

$\Delta\delta^{18}O$ record (between *G. ruber* and *G. truncatulinoides*) whose variations have been attributed mainly to main thermocline temperature changes (Nascimento et al., 2021b). These differences between the temperature of the upper (TEX$^H_{86}$-SubT) and

280   main thermocline (Mg/Ca-ThT) are attributed to different mechanisms controlling subsurface variations within distinct layers of the thermocline. The South Atlantic Central Waters are cold and nutrient rich intermediate waters underlying the warm tropical waters as observed in local vertical nutrient profiles (Supplementary materials, Figure S4). The high nutrient concentrations in the lower half of the thermocline while tropical surface waters are nutrient-poor indicate the vertical incursions of SACW up to the main thermocline. Such SACW incursions into the thermocline have been reported along

285   Brazilian margins, in response to ocean-atmosphere dynamics, mainly associated with wind and coastal upwelling on the west margin (Gérikas Ribeiro et al., 2016; Lessa et al., 2016). We suggest here that in contrast to G. truncatulinoides, the TEX$^H_{86}$ records the temperature of the upper thermocline which is not under the influence of SACW.

    The observed deglacial warming are common features attributed, as for the Termination I, to the accumulation of warm waters in the South Atlantic during times of weakened AMOC. A similar thermal evolution is observed here within GL-1180

290   temperature records during the Termination III, indicating a recurring feature in this region for at least the last 3 deglaciations. In addition, the GL-1180 upper thermocline temperature records exhibit significant increases during the transition from "cold" (MIS 7d and 7b) to "warm" (MIS 7c and 7a) sub-stages of the MIS 7 but with smaller amplitude of changes compared to the deglaciations (Figure 3). Regarding to the previous assumptions, these "sub-deglaciations" are smaller analogous to the deglaciations, driven by similar mechanisms.

295   Two principal climatic processes can explain the deglacial temperature changes observed within the western South Atlantic: (i) the thermodynamic model of the bipolar seesaw (Broecker et al., 1990) which was proposed to explain the opposite thermal behaviour between the (cooling) North and the (warming) South Atlantic during periods of reduced AMOC (see 1. Introduction; Pedro et al., 2018) and (ii) the increase in Agulhas Leakage outflow during deglaciations of the Late Pleistocene (Peeters et al., 2004), suggested to be responsible of large inputs of saline and warm waters to the South Atlantic (Scussolini

300   et al., 2015). The upper ocean warming recorded by the GL-1180 temperature record during the past 3 glacial terminations, at the extreme north-western boundary of the South Atlantic, could be explained by one (bipolar seesaw) or the other (Agulhas

Leakage) hypothesis, or both of them. We investigated subsequently which of these hypotheses is the most likely to explain the water temperature variations observed in the western South Atlantic.

4.2 Bipolar seesaw influence on millennial-scale changes in upper western tropical Atlantic temperature

305   As suggested above, the upper ocean warming observed in core GL-1180 during the last three glacial terminations could be due (at least partly) to the thermal bipolar seesaw concept, an interhemispheric coupling in response to millennial-scale abrupt climatic events related to AMOC changes (Broecker et al., 1990; Crowley, 1992; Stocker and Johnsen, 2003). To fully assess the impact of millennial-scale abrupt events on the upper western Atlantic temperature, we examined the variations in GL-1180 temperature record over millennial-scale climatic events (Figure 5). We focus here on the upper thermocline record

310   ($TEX^{H'}_{86}$-SubT), which exhibits larger variations compared to the $U^{K'}_{37}$-SST, and investigate the period between ~70 and 125 kyr BP, which has a higher temporal resolution than the last glacial period. Within our age model uncertainties (Nascimento et al., 2021b), a subsurface warming (+ 2.5°C on average) is observed at 74, 84 and 107 kyr BP corresponding to Greenland Stadials (GS), i.e. cold phases of DO cycles (Rasmussen et al., 2014) 20, 22 and 25, respectively (Figure 5E). During these periods of cold North Atlantic (Martrat et al., 2007) and weakened AMOC (McManus et al., 2004; Piotrowski et al., 2005),

315   the western tropical Atlantic experienced water mass ventilation (Waelbroeck et al., 2018), stratification (Venancio et al., 2018) and upper ocean temperature changes (Jaeschke et al., 2007; Portilho-Ramos et al., 2017; Rama-Corredor et al., 2015) (Figures 5B, C, D). Within the main thermocline, the temperature record (Mg/Ca-ThT) of GL-1090 core (Santos et al., 2020) exhibits a seawater warming during GS19, GS20 and GS21 (Figure 5F). In addition, the Mg/Ca-ThT record of GL-1180 core (Nascimento et al., 2021b) also shows a temperature increase during GS20 (Figure 5G). Both warmings were induced by the

320   reduced meridional heat transport and the accumulation of warm waters within the South Atlantic basin during such periods.

    Based on the bipolar seesaw model (Stocker and Johnsen, 2003), the extension of sea-ice cover and the reduction of deep-water formation in the Nordic seas (Boers et al., 2018) led to a reduction of the interhemispheric northward heat advection and thus, to a warming of the South Atlantic basin (Landais et al., 2015), as observed in GL-1180 and GL-1090 temperature records. This thermal response is also well represented by freshwater hosing model experiments, i.e. forcing the reduction of

325   deep water formation in the Nordic seas by large inputs of freshwater within the North Atlantic (Chang et al., 2008). The AMOC collapse leads to the accumulation of warm waters (Dahl et al., 2005) in the South and tropical Atlantic because of the

reduction of the cross-equatorial North Brazil Current transport, especially at thermocline levels (Laurian and Drijfhout, 2011), thus inducing the upper thermocline warming (TEX$^H_{86}$-SubT) observed in the GL-1180 core (Figure 5E).

During glacial terminations, the occurrence of millennial-scale events, i.e. Heinrich events, led to a substantial warming of the South Atlantic as explained by the thermal bipolar seesaw model. Nevertheless, the upper thermocline temperature record of GL-1180 core exhibits an increase of +2°C during Greenland Stadials which accounts only for the half of the deglacial warming (Figures 3, Figure 5). Thus, we cannot exclude that the bipolar see saw is responsible for, at least, part of the observed temperature increase during glacial terminations (Barker and Diz, 2014). However, deglaciations of the late Pleistocene are also associated with an increase of the Agulhas Leakage outflow, a major contributor of warm and saline thermocline waters to the South Atlantic (Peeters et al., 2004). Assuming the role of the bipolar seesaw in the upper ocean warming in the western tropical Atlantic, we therefore investigate the potential of Agulhas Leakage waters to explain these temperature increases.

4.3 Impact on western tropical Atlantic upper ocean temperatures of the expansion of Agulhas Leakage waters during past terminations

In the GL-1180 core, the difference between the U$^{K'}_{37}$-SST and TEX$_{86}$-SubT temperatures (vertical gradient, ΔST, Figure 5C) exhibited minimal values over the last three deglaciations. A similar decrease in the vertical thermal contrast between the mixed layer and the upper thermocline over glacial terminations of the late Pleistocene is also observed in U$^{K'}_{37}$ and TEX$^H_{86}$ temperature records from cores collected within the Agulhas Current pathway along southern Africa (Caley et al., 2011; Figures 5A, B) and in the Cape Basin (Cartagena- Sierra et al., 2021). A similar deglacial temperature pattern was previously reported in the Cape Basin records (CBR cores, Figure 5D) (Peeters et al., 2004). Deglaciations are associated with an increase in the Agulhas Leakage, which is the outflow of warm and saline waters from the Agulhas Current in the South Atlantic (Nirmal et al., 2023; Peeters et al., 2004) (Figure 5E). The intensity of the Agulhas Leakage strongly depends on the position of the southern hemisphere mid-latitude westerlies (Biastoch et al., 2009). This wind belt related with the subtropical front exhibits latitudinal migrations over orbital (Bard and Rickaby, 2009) and longer timescales (Cartagena- Sierra et al., 2021). During full glacial states, these westerlies were suggested to blow at a latitude of ~35°S in the Cape Basin region (Bard and Rickaby, 2009), therefore blocking the Agulhas Leakage outflow in the South Atlantic. At the onset of the deglaciation, the poleward shift of the mid-latitude westerlies initiates the leakage of the Agulhas Current, i.e. the outflow of these warm and

salty waters, to the South Atlantic. These waters then spread in the South Atlantic and mixed with South Atlantic central waters, imprinting their physical properties, high salinity (Scussolini et al., 2015), high temperatures (Kasper et al., 2014) and low vertical gradient (ΔST, Figure 5A) over the South Atlantic.

355   The changes in Agulhas Leakage outflow have first been reconstructed using subtropical foraminiferal assemblages (Peeters et al., 2004) including *G. menardii,* which is transported by Agulhas waters outflow from the Indian Ocean to the South Atlantic (Caley et al., 2014). On the western side of the South Atlantic, an increase in *G. menardii* abundance was also observed during Termination I (Santos et al., 2014) and imputed to the spreading of Agulhas Leakage warm and salty waters. The increase outflow of Agulhas waters during glacial terminations has also been suggested to explain the increase in upper

360   ocean temperature and salinity reconstructed in the western South Atlantic during TII (Ballalai et al., 2019) and the eastern South Atlantic during TI and TII (Kasper et al., 2014; Scussolini et al., 2015). Agulhas warm and salty mode waters are spreading into the South Atlantic mainly within the thermocline (Guerra et al., 2022), and constitute the main source of heat and salt to the upper limb layers of this basin (Castellanos et al., 2017). The abovementioned records reported a stronger temperature and salinity increase at upper (Kasper et al., 2014) and permanent thermocline (Ballalai et al., 2019; Scussolini et

365   al., 2015) levels compared to the surface.

     Similarly, the temperature increase recorded in core GL-1180 during deglaciations has a higher amplitude in the upper thermocline (+ 5°C) than in surface (+2°C) water. In addition, the upper thermocline temperature maximum is reached during the glacial termination, while, at the surface, the temperature remains relatively high during the later interglacial. Upstream, the same temperature pattern was reported in the Mozambique Channel (Caley et al., 2011), and in the Southeast Atlantic

370   (Kasper et al., 2014; Peeters et al., 2004).

     Therefore, these results indicate that the signature of Agulhas Leakage waters was observed during past glacial terminations along their pathway from the Indian Ocean to the western boundary of the South Atlantic through the Cape Basin. In addition, Agulhas Leakage waters were reported to reach the western South Atlantic on modern times (Castellanos et al., 2017; Guerra et al., 2022; Lübbecke et al., 2015) and over past deglaciations (Ballalai et al., 2019; Santos et al., 2014). Altogether, these

375   observations suggest that the upper ocean warming in the western tropical Atlantic during the last three glacial terminations is due, at least partly, to the spreading of Agulhas Leakage waters in the South Atlantic.

4.4 Proposed mechanisms to explain the upper western tropical Atlantic warming during the last 3 glacial terminations

The warming of western tropical Atlantic subsurface waters occurred, at the onset of deglaciations (~19, ~135 and ~251 kyr BP respectively for TI, TII and TIII) with a large amplitude (+ 3 to + 5°C), especially at the upper thermocline, in a relatively short time interval (< 2 kyr) indicating the advection of considerable volumes of warm waters (Figure 7). A similar temperature pattern was also reported within the Mozambique Channel (Caley et al., 2011) and in the southeastern South Atlantic (Kasper et al., 2014), on the course of the cross-oceanic Agulhas Leakage (Figure 7). As discussed in section 4.3, the poleward shift of the southern westerlies at the onset of the deglaciation led to massive outflow of Indo-Pacific waters in the South Atlantic (Bard and Rickaby, 2009; Peeters et al., 2004). During the preceding glacial period, Indian Ocean waters were circulating in closed system because of the latitude of the southern westerlies (Beal et al., 2011), increasing gradually their heat (Sun et al., 2022) and salt contents. The millennial-scale and large increase observed in these temperature records is a consequence of the progressive advection and accumulation of these waters, especially at thermocline levels (Guerra et al., 2022) in the South Atlantic (Figure 8, left panel). In the South Atlantic, the subtropical gyre was suggested to intensify during deglaciations (Laurian and Drijfhout, 2011), concomitantly with a (i) a southward migration of the ITCZ, (ii) an intensification of the SE trades and (iii) a reduction of the cross-equatorial North Brazil Current in response to large iceberg discharges in the North Atlantic (Nace et al., 2014). These mechanisms allowed for the accumulation of warm and salty waters in the whole South Atlantic basin up to tropical latitudes (Figure 8), thus explaining the pattern observed in temperature records on eastern and western boundaries of the South Atlantic (Figures 4, 7). The restricted transport by Agulhas rings and eddies on short timescales (Guerra et al., 2022; Wang et al., 2015) would require, during deglaciations, centuries to millennia to spread the Agulhas heat over the whole South Atlantic at thermocline and intermediate levels and warm this basin as indicated by temperature records along Brazilian margins (Figure 4).

In addition, a similar temperature pattern, i.e. surface and subsurface deglacial warmings, was reported in the tropical North Atlantic, thus indicating the spreading of these warm waters across the equator (Lopes dos Santos et al., 2010; Reißig et al., 2019; Schmidt et al., 2012) (Figure 7). However, the main cross-equatorial upper ocean current in the Atlantic i.e. the North Brazil Current was suggested to strongly slowdown (Laurian and Drijfhout, 2011) during abrupt AMOC collapses of the last

17

deglaciation (Arz et al., 1999; Bahr et al., 2018; Weldeab et al., 2006). In parallel, because the North Atlantic is cold during AMOC reduction events of glacial terminations, the eastward and cross-equatorial advection of the above-mentioned warm waters is required to explain the mirrored temperature pattern observed on the western (GL-1180 core, this study) and eastern (GeoB9528-3 core, Lopes dos Santos et al., 2010) sides of the tropical Atlantic (Figure 7).

We propose here a schematic overview of surface and thermocline circulations in the tropical Atlantic to shed light on the main currents and associated temperature patterns (Figure 8). During the deglaciation, the advection of warm waters from the Indo-Pacific basins warmed the South Atlantic in response to the increase of the Agulhas Leakage. In addition, the reduced cross-equatorial AMOC transport led to the accumulation of these warm waters within the South Atlantic. The South Atlantic basin warmed up, while the North Atlantic cooled during events of meltwater input and AMOC reduction, thus establishing a strong interhemispheric SST dipole in the Atlantic. The combined action of these processes over the deglaciation leads to the development of this tropical SST dipole during several millennia and maintains favourable conditions for reorganizations in the wind fields, associated surface currents and subsurface heat storages (Joyce et al., 2004; Figure 8, right panel), as observed nowadays (Chang et al., 1997; Lee and Wang, 2008). In response to the increased cross-equatorial temperature gradient, a stronger than normal cross-equatorial gyre develops (Laurian and Drijfhout, 2011). It is characterized by changes in upper ocean circulation in response to wind stresses (Joyce et al., 2004; Wu et al., 2008), with the formation of a westerly wind anomaly on the western part of the tropical Atlantic. The SST anomaly strengthens, alimented by Bjerknes-type feedbacks observed on decadal timescales, and sustains these wind stresses (Lee and Wang, 2008). Together with the reduction of the North Brazil Current (Nace et al., 2014), these tropical westerlies would promote a prominent eastward current (Xie et al., 1999), probably an analogous of the North Brazil Current retroflection, which is a precursor of the North Equatorial Countercurrent. This seasonal retroflection (Lumpkin and Garzoli, 2005) was at least prolonged over the year or even stronger (Bahr et al., 2018; Vink et al., 2001) and persistent in response to the weakening of the North Brazil Current (Wilson et al., 2011) (Figure 8). An enhanced North Equatorial Countercurrent, propagating rings and eddies within the upper layers (Lumpkin and Garzoli, 2005; Schott et al., 1995), crossed zonally the tropical Atlantic to its eastern boundary and diverged towards the African continent. Its southward branch re-circulated in the South Atlantic, while its northward one supplied warm waters to the eastern tropical North Atlantic (Meier et al., 2021). Finally, the strengthened northeast trades dragged these warm

18

waters westward and limited their northward spreading into the North Atlantic. Existing records in the eastern (GeoB9528-3, Lopes dos Santos et al., 2010) and western (SO164-03-4, M78/1-235-1, VM12-107 Reißig et al., 2019; Schmidt et al., 2012) tropical North Atlantic exhibiting a pronounced surface and subsurface warming over glacial terminations indicates the

430 propagation of South Atlantic waters, although interhemispheric upper ocean transport is reduced (Laurian and Drijfhout, 2011) (Figure 8). These South Atlantic waters spreaded meridionally and zonally within the tropical Atlantic, through mode waters at thermocline and intermediate levels (Guerra et al., 2022; Laurian and Drijfhout, 2011), explaining the large accumulation of warm waters up to 20°N (Schmidt et al., 2012; Weldeab et al., 2006). Due to air-sea interactions, the atmospheric and oceanic reorganizations greatly impact the heat transport in the tropical thermocline (Laurian and Drijfhout,

435 2011; Xie et al., 1999). At the end of the deglacial interval, the resumption of the AMOC and northward upper ocean transport drained out warm waters, especially at thermocline levels, explaining the subsurface i.e. upper thermocline sharp cooling (compared to the surface) observed in the low-latitude temperature records (Lopes dos Santos et al., 2010; Reißig et al., 2019; Schmidt et al., 2012) including those of GL-1180.

5. Conclusions

440 In this study, the past upper ocean temperature (mixed layer i.e. surface, and upper thermocline i.e. subsurface) in the western tropical Atlantic were reconstructed over the last 305 kyr using organic temperature proxies, $U^{K'}_{37}$ and TEX^H_{86} respectively. Besides a glacial-interglacial variability, the temperature records exhibited increases over the last 3 deglaciations especially at subsurface levels. Similar deglacial warmings were previously reported on the Brazilian margins and in the southeastern South Atlantic. The accumulation of warm waters in the whole South Atlantic basin were attributed, at least

445 partly, to the reduction of the meridional cross-equatorial heat transport linked with deglacial Heinrich events. Nevertheless, the large magnitude of the subsurface warming is suggested here to be also due to the spreading, into the South Atlantic, of the Agulhas Leakage warm and salty waters in response to the poleward shift of the southern westerlies. These mode waters are propagating especially at thermocline level and were accumulating into the South Atlantic with the intensified subtropical gyre during deglacial periods. In addition, we attributed the interhemispheric spreading of these waters on the eastern and

450 western tropical North Atlantic to the development of a cross-equatorial gyre in parallel of the reduction of the transport by

the North Brazil Current. This gyre exhibits a strong eastward upper ocean current responding to an anomalous wind stress and allow the expansion of South Atlantic warm waters to the eastern boundary of the tropical North Atlantic during, at least, the last three glacial terminations of the Late Pleistocene.

Competing interests

455   The authors declare that they have no known competing financial interests or personal relationships that could have appeared to influence the work reported in this paper.

References

470   Arz, H.W., Pätzold, J., Wefer, G., 1999. The deglacial history of the western tropical Atlantic as inferred from high resolution stable isotope records off northeastern Brazil. Earth and Planetary Science Letters 167, 105–117. https://doi.org/10.1016/S0012-821X(99)00025-4

Bahr, A., Hoffmann, J., Schönfeld, J., Schmidt, M.W., Nürnberg, D., Batenburg, S.J., Voigt, S., 2018. Low-latitude expressions of high-latitude forcing during Heinrich Stadial 1 and the Younger Dryas in northern South America. Global and
475   Planetary Change 160, 1–9. https://doi.org/10.1016/j.gloplacha.2017.11.008

Ballalai, J.M., Santos, T.P., Lessa, D.O., Venancio, I.M., Chiessi, C.M., Johnstone, H.J.H., Kuhnert, H., Claudio, M.R., Toledo, F., Costa, K.B., Albuquerque, A.L.S., 2019. Tracking Spread of the Agulhas Leakage Into the Western South Atlantic and Its Northward Transmission During the Last Interglacial. Paleoceanography and Paleoclimatology 34, 1744–1760. https://doi.org/10.1029/2019PA003653

480   Bard, E., Rickaby, R.E.M., 2009. Migration of the subtropical front as a modulator of glacial climate. Nature 460, 380–383. https://doi.org/10.1038/nature08189

Barker, S., Diz, P., 2014. Timing of the descent into the last Ice Age determined by the bipolar seesaw. Paleoceanography 29, 489–507. https://doi.org/10.1002/2014PA002623

Beal, L.M., De Ruijter, W.P.M., Biastoch, A., Zahn, R., SCOR/WCRP/IAPSO Working Group 136, Cronin, M., Hermes, J.,
485   Lutjeharms, J., Quartly, G., Tozuka, T., Baker-Yeboah, S., Bornman, T., Cipollini, P., Dijkstra, H., Hall, I., Park, W., Peeters, F., Penven, P., Ridderinkhof, H., Zinke, J., 2011. On the role of the Agulhas system in ocean circulation and climate. Nature 472, 429–436. https://doi.org/10.1038/nature09983

Behling, H., W. Arz, H., Pätzold, J., Wefer, G., 2000. Late Quaternary vegetational and climate dynamics in northeastern Brazil, inferences from marine core GeoB 3104-1. Quaternary Science Reviews 19, 981–994.
490   https://doi.org/10.1016/S0277-3791(99)00046-3

Benthien, A., Müller, P.J., 2000. Anomalously low alkenone temperatures caused by lateral particle and sediment transport in the Malvinas Current region, western Argentine Basin. Deep Sea Research Part I: Oceanographic Research Papers 47, 2369–2393. https://doi.org/10.1016/S0967-0637(00)00030-3

Biastoch, A., Böning, C.W., Schwarzkopf, F.U., Lutjeharms, J.R.E., 2009. Increase in Agulhas leakage due to poleward shift
495   of Southern Hemisphere westerlies. Nature 462, 495–498. https://doi.org/10.1038/nature08519

Blaauw, M., Christen, J.A., 2011. Flexible paleoclimate age-depth models using an autoregressive gamma process. Bayesian Analysis 6, 457–474. https://doi.org/10.1214/11-BA618

Boers, N., Ghil, M., Rousseau, D.-D., 2018. Ocean circulation, ice shelf, and sea ice interactions explain Dansgaard–Oeschger cycles. Proceedings of the National Academy of Sciences 115. https://doi.org/10.1073/pnas.1802573115

500   Bond, G., Heinrich, H., Broecker, W., Labeyrie, L., McManus, J., Andrews, J., Huon, S., Jantschik, R., Clasen, S., Simet, C., Tedesco, K., Klas, M., Bonani, G., Ivy, S., 1992. Evidence for massive discharges of icebergs into the North Atlantic ocean during the last glacial period. Nature 360, 245–249. https://doi.org/10.1038/360245a0

Broecker, W.S., Bond, G., Klas, M., Bonani, G., Wolfli, W., 1990. A salt oscillator in the glacial Atlantic? 1. The concept. Paleoceanography 5, 469–477. https://doi.org/10.1029/PA005i004p00469

505   Buckley, M.W., Marshall, J., 2016. Observations, inferences, and mechanisms of the Atlantic Meridional Overturning Circulation: A review. Reviews of Geophysics 54, 5–63. https://doi.org/10.1002/2015RG000493

Caley, T., Kim, J.-H., Malaizé, B., Giraudeau, J., Laepple, T., Caillon, N., Charlier, K., Rebaubier, H., Rossignol, L., Castañeda, I.S., Schouten, S., Sinninghe Damsté, J.S., 2011. High-latitude obliquity as a dominant forcing in the Agulhas current system. Climate of the Past 7, 1285–1296. https://doi.org/10.5194/cp-7-1285-2011

510   Caley, T., Peeters, F.J.C., Biastoch, A., Rossignol, L., van Sebille, E., Durgadoo, J., Malaizé, B., Giraudeau, J., Arthur, K., Zahn, R., 2014. Quantitative estimate of the paleo-Agulhas leakage. Geophysical Research Letters 41, 1238–1246. https://doi.org/10.1002/2014GL059278

Cartagena- Sierra, A., Berke, M.A., Robinson, R.S., Marcks, B., Castañeda, I.S., Starr, A., Hall, I.R., Hemming, S.R., LeVay, L.J., Expedition 361 Scientific Party, 2021. Latitudinal Migrations of the Subtropical Front at the Agulhas Plateau
515   Through the Mid- Pleistocene Transition. Paleoceanog and Paleoclimatol 36. https://doi.org/10.1029/2020PA004084

Castañeda, I.S., Mulitza, S., Schefuß, E., Lopes dos Santos, R.A., Sinninghe Damsté, J.S., Schouten, S., 2009. Wet phases in the Sahara/Sahel region and human migration patterns in North Africa. Proceedings of the National Academy of Sciences 106, 20159–20163. https://doi.org/10.1073/pnas.0905771106

520 Castellanos, P., Campos, E.J.D., Piera, J., Sato, O.T., Dias, M.A.F.S., 2017. Impacts of Agulhas Leakage on the Tropical Atlantic Western Boundary Systems. Journal of Climate 30, 6645–6659. https://doi.org/10.1175/JCLI-D-15-0878.1

Ceccopieri, M., Carreira, R.S., Wagener, A.L.R., Hefter, J.H., Mollenhauer, G., 2018. On the application of alkenone- and GDGT-based temperature proxies in the south-eastern Brazilian continental margin. Organic Geochemistry 126, 43–56. https://doi.org/10.1016/j.orggeochem.2018.10.009

Chang, P., Ji, L., Li, H., 1997. A decadal climate variation in the tropical Atlantic Ocean from the thermodynamic air-sea
525 interactions. Nature 385, 516–518. https://doi.org/10.1038/385516a0

Chang, P., Zhang, R., Hazeleger, W., Wen, C., Wan, X., Ji, L., Haarsma, R.J., Breugem, W.-P., Seidel, H., 2008. Oceanic link between abrupt changes in the North Atlantic Ocean and the African monsoon. Nature Geoscience 1, 444–448. https://doi.org/10.1038/ngeo218

Chiessi, C.M., Mulitza, S., Mollenhauer, G., Silva, J.B., Groeneveld, J., Prange, M., 2015. Thermal evolution of the western
530 South Atlantic and the adjacent continent during Termination 1. Clim. Past 11, 915–929. https://doi.org/10.5194/cp-11-915-2015

Chiessi, C.M., Mulitza, S., Paul, A., Pätzold, J., Groeneveld, J., Wefer, G., 2008. South Atlantic interocean exchange as the trigger for the Bølling warm event. Geology 36, 919. https://doi.org/10.1130/G24979A.1

Conte, M.H., Sicre, M.-A., Rühlemann, C., Weber, J.C., Schulte, S., Schulz-Bull, D., Blanz, T., 2006. Global temperature
535 calibration of the alkenone unsaturation index (UK′37) in surface waters and comparison with surface sediments. Geochemistry, Geophysics, Geosystems 7, n/a-n/a. https://doi.org/10.1029/2005GC001054

Cordeiro, T.A., Brandini, F.P., Rosa, R.S., Sassi, R., 2013. Deep Chlorophyll Maximum in Western Equatorial Atlantic - How does it Interact with Islands Slopes and Seamounts? Marine Science 3, 30–37. https://doi.org/10.5923/j.ms.20130301.03

540 Crivellari, S., Chiessi, C.M., Kuhnert, H., Häggi, C., Mollenhauer, G., Hefter, J., Portilho-Ramos, R., Schefuß, E., Mulitza, S., 2019. Thermal response of the western tropical Atlantic to slowdown of the Atlantic Meridional Overturning Circulation. Earth and Planetary Science Letters 519, 120–129. https://doi.org/10.1016/j.epsl.2019.05.006

Crowley, T.J., 1992. North Atlantic Deep Water cools the southern hemisphere. Paleoceanography 7, 489–497. https://doi.org/10.1029/92PA01058

545 Dahl, K.A., Broccoli, A.J., Stouffer, R.J., 2005. Assessing the role of North Atlantic freshwater forcing in millennial scale climate variability: a tropical Atlantic perspective. Climate Dynamics 24, 325–346. https://doi.org/10.1007/s00382-004-0499-5

Dauner, A.L.L., Mollenhauer, G., Bícego, M.C., de Souza, M.M., Nagai, R.H., Figueira, R.C.L., de Mahiques, M.M., Sousa, S.H. de M. e, Martins, C.C., 2019. Multi-proxy reconstruction of sea surface and subsurface temperatures in the
550 western South Atlantic over the last ~75 kyr. Quaternary Science Reviews 215, 22–34. https://doi.org/10.1016/j.quascirev.2019.04.020

Deaney, E.L., Barker, S., van de Flierdt, T., 2017. Timing and nature of AMOC recovery across Termination 2 and magnitude of deglacial CO2 change. Nature Communications 8, 14595. https://doi.org/10.1038/ncomms14595

Denton, G.H., Anderson, R.F., Toggweiler, J.R., Edwards, R.L., Schaefer, J.M., Putnam, A.E., 2010. The Last Glacial
555 Termination. Science 328, 1652–1656. https://doi.org/10.1126/science.1184119

Durgadoo, J.V., Loveday, B.R., Reason, C.J.C., Penven, P., Biastoch, A., 2013. Agulhas Leakage Predominantly Responds to the Southern Hemisphere Westerlies. Journal of Physical Oceanography 43, 2113–2131. https://doi.org/10.1175/JPO-D-13-047.1

Gérikas Ribeiro, C., Lopes dos Santos, A., Marie, D., Helena Pellizari, V., Pereira Brandini, F., Vaulot, D., 2016. Pico and
560 nanoplankton abundance and carbon stocks along the Brazilian Bight. PeerJ 4, e2587. https://doi.org/10.7717/peerj.2587

Goes, M., Molinari, R., da Silveira, I., Wainer, I., 2005. Retroflections of the North Brazil Current during February 2002. Deep Sea Research Part I: Oceanographic Research Papers 52, 647–667. https://doi.org/10.1016/j.dsr.2004.10.010

Guerra, L.A.A., Mill, G.N., Paiva, A.M., 2022. Observing the spread of Agulhas Leakage into the Western South Atlantic by
565 tracking mode waters within ocean rings. Front. Mar. Sci. 9, 958733. https://doi.org/10.3389/fmars.2022.958733

Heinrich, H., 1988. Origin and consequences of cyclic ice rafting in the Northeast Atlantic Ocean during the past 130,000 years. Quaternary Research 29, 142–152. https://doi.org/10.1016/0033-5894(88)90057-9

Hopmans, E.C., Schouten, S., Sinninghe Damsté, J.S., 2016. The effect of improved chromatography on GDGT-based palaeoproxies. Organic Geochemistry 93, 1–6. https://doi.org/10.1016/j.orggeochem.2015.12.006

570   Hopmans, E.C., Weijers, J.W.H., Schefuß, E., Herfort, L., Sinninghe Damsté, J.S., Schouten, S., 2004. A novel proxy for terrestrial organic matter in sediments based on branched and isoprenoid tetraether lipids. Earth and Planetary Science Letters 224, 107–116. https://doi.org/10.1016/j.epsl.2004.05.012

Huguet, A., Coffinet, S., Roussel, A., Gayraud, F., Anquetil, C., Bergonzini, L., Bonanomi, G., Williamson, D., Majule, A., Derenne, S., 2019. Evaluation of 3-hydroxy fatty acids as a pH and temperature proxy in soils from temperate and

575   tropical altitudinal gradients. Organic Geochemistry 129, 1–13. https://doi.org/10.1016/j.orggeochem.2019.01.002

Huguet, C., Hopmans, E.C., Febo-Ayala, W., Thompson, D.H., Sinninghe Damsté, J.S., Schouten, S., 2006. An improved method to determine the absolute abundance of glycerol dibiphytanyl glycerol tetraether lipids. Organic Geochemistry 37, 1036–1041. https://doi.org/10.1016/j.orggeochem.2006.05.008

Hurley, S.J., Lipp, J.S., Close, H.G., Hinrichs, K.-U., Pearson, A., 2018. Distribution and export of isoprenoid tetraether lipids

580   in suspended particulate matter from the water column of the Western Atlantic Ocean. Organic Geochemistry 116, 90–102. https://doi.org/10.1016/j.orggeochem.2017.11.010

Inglis, G.N., Farnsworth, A., Lunt, D., Foster, G.L., Hollis, C.J., Pagani, M., Jardine, P.E., Pearson, P.N., Markwick, P., Galsworthy, A.M.J., Raynham, L., Taylor, Kyle.W.R., Pancost, R.D., 2015. Descent toward the Icehouse: Eocene sea surface cooling inferred from GDGT distributions. Paleoceanography 30, 1000–1020.

585   https://doi.org/10.1002/2014PA002723

Inglis, G.N., Tierney, J.E., 2020. The TEX86 Paleotemperature Proxy, 1st ed. Cambridge University Press. https://doi.org/10.1017/9781108846998

Jaeschke, A., Rühlemann, C., Arz, H., Heil, G., Lohmann, G., 2007. Coupling of millennial-scale changes in sea surface temperature and precipitation off northeastern Brazil with high-latitude climate shifts during the last glacial period.

590   Paleoceanography 22, n/a-n/a. https://doi.org/10.1029/2006PA001391

Joyce, T.M., Frankignoul, C., Yang, J., Phillips, H.E., 2004. Ocean Response and Feedback to the SST Dipole in the Tropical Atlantic*. Journal of Physical Oceanography 34, 2525–2540. https://doi.org/10.1175/JPO2640.1

Kageyama, M., Paul, A., Roche, D.M., Van Meerbeeck, C.J., 2010. Modelling glacial climatic millennial-scale variability related to changes in the Atlantic meridional overturning circulation: a review. Quaternary Science Reviews 29, 2931–

595   2956. https://doi.org/10.1016/j.quascirev.2010.05.029

Kasper, S., van der Meer, M.T.J., Mets, A., Zahn, R., Sinninghe Damsté, J.S., Schouten, S., 2014. Salinity changes in the Agulhas leakage area recorded by stable hydrogen isotopes of C37 alkenones during Termination I and II. Climate of the Past 10, 251–260. https://doi.org/10.5194/cp-10-251-2014

Kim, J.-H., Schneider, R.R., 2003. Low-latitude control of interhemispheric sea-surface temperature contrast in the tropical

600   Atlantic over the past 21 kyears: the possible role of SE trade winds. Climate Dynamics 21, 337–347. https://doi.org/10.1007/s00382-003-0341-5

Kim, J.-H., Schouten, S., Hopmans, E.C., Donner, B., Sinninghe Damsté, J.S., 2008. Global sediment core-top calibration of the TEX86 paleothermometer in the ocean. Geochimica et Cosmochimica Acta 72, 1154–1173. https://doi.org/10.1016/j.gca.2007.12.010

605   Kim, J.-H., van der Meer, J., Schouten, S., Helmke, P., Willmott, V., Sangiorgi, F., Koç, N., Hopmans, E.C., Damsté, J.S.S., 2010. New indices and calibrations derived from the distribution of crenarchaeal isoprenoid tetraether lipids: Implications for past sea surface temperature reconstructions. Geochimica et Cosmochimica Acta 74, 4639–4654. https://doi.org/10.1016/j.gca.2010.05.027

Knorr, G., Lohmann, G., 2007. Rapid transitions in the Atlantic thermohaline circulation triggered by global warming and

610   meltwater during the last deglaciation. Geochemistry, Geophysics, Geosystems 8. https://doi.org/10.1029/2007GC001604

Krelling, A.P.M., Silveira, I.C.A., Polito, P.S., Gangopadhyay, A., Martins, R.P., Lima, J.A.M., Marin, F.D.O., 2020. A Newly Observed Quasi- stationary Subsurface Anticyclone of the North Brazil Undercurrent at 4°S: The Potiguar Eddy. J. Geophys. Res. Oceans 125. https://doi.org/10.1029/2020JC016268

615 Landais, A., Masson-Delmotte, V., Stenni, B., Selmo, E., Roche, D.M., Jouzel, J., Lambert, F., Guillevic, M., Bazin, L., Arzel, O., Vinther, B., Gkinis, V., Popp, T., 2015. A review of the bipolar see–saw from synchronized and high resolution ice core water stable isotope records from Greenland and East Antarctica. Quaternary Science Reviews 114, 18–32. https://doi.org/10.1016/j.quascirev.2015.01.031

Latasa, M., Cabello, A.M., Morán, X.A.G., Massana, R., Scharek, R., 2017. Distribution of phytoplankton groups within the
620 deep chlorophyll maximum: Distribution of phytoplankton groups in the DCM. Limnology and Oceanography 62, 665–685. https://doi.org/10.1002/lno.10452

Laurian, A., Drijfhout, S.S., 2011. Response of the South Atlantic circulation to an abrupt collapse of the Atlantic meridional overturning circulation. Climate Dynamics 37, 521–530. https://doi.org/10.1007/s00382-010-0890-3

Lee, S.-K., Wang, C., 2008. Tropical Atlantic Decadal Oscillation and Its Potential Impact on the Equatorial Atmosphere–
625 Ocean Dynamics: A Simple Model Study. Journal of Physical Oceanography 38, 193–212. https://doi.org/10.1175/2007JPO3450.1

Lessa, D.V., Venancio, I.M., Dos Santos, T.P., Belem, A.L., Turcq, B.J., Sifeddine, A., Albuquerque, A.L.S., 2016. Holocene oscillations of Southwest Atlantic shelf circulation based on planktonic foraminifera from an upwelling system (off Cabo Frio, Southeastern Brazil). The Holocene 26, 1175–1187. https://doi.org/10.1177/0959683616638433

630 Li, D., Zhao, M., Tian, J., Li, L., 2013. Comparison and implication of TEX86 and U37K' temperature records over the last 356kyr of ODP Site 1147 from the northern South China Sea. Palaeogeography, Palaeoclimatology, Palaeoecology 376, 213–223. https://doi.org/10.1016/j.palaeo.2013.02.031

Lisiecki, L.E., Raymo, M.E., 2005. A Pliocene-Pleistocene stack of 57 globally distributed benthic δ^{18}O records: PLIOCENE-PLEISTOCENE BENTHIC STACK. Paleoceanography 20, n/a-n/a. https://doi.org/10.1029/2004PA001071

635 Liu, W., Fedorov, A.V., Xie, S.-P., Hu, S., 2020. Climate impacts of a weakened Atlantic Meridional Overturning Circulation in a warming climate. Science Advances 6, eaaz4876. https://doi.org/10.1126/sciadv.aaz4876

Locarnini, R.A., Mishonov, A.V., Antonov, John I., Boyer, Timothy P., Garcia, H.E., Baranova, Olga K., Zweng, M.M., Paver, C.R., Reagan, James R., Johnson, D.R., Seidov, D., 2013. World Ocean Atlas 2013 Volume 1: Temperature. NOAA Atlas NESDIS 73 40.

640 Lopes dos Santos, R.A., Prange, M., Castañeda, I.S., Schefuß, E., Mulitza, S., Schulz, M., Niedermeyer, E.M., Sinninghe Damsté, J.S., Schouten, S., 2010. Glacial–interglacial variability in Atlantic meridional overturning circulation and thermocline adjustments in the tropical North Atlantic. Earth and Planetary Science Letters 300, 407–414. https://doi.org/10.1016/j.epsl.2010.10.030

Lübbecke, J.F., Durgadoo, J.V., Biastoch, A., 2015. Contribution of Increased Agulhas Leakage to Tropical Atlantic Warming.
645 Journal of Climate 28, 9697–9706. https://doi.org/10.1175/JCLI-D-15-0258.1

Lumpkin, R., Garzoli, S.L., 2005. Near-surface circulation in the Tropical Atlantic Ocean. Deep Sea Research Part I: Oceanographic Research Papers 52, 495–518. https://doi.org/10.1016/j.dsr.2004.09.001

Lynch-Stieglitz, J., 2017. The Atlantic Meridional Overturning Circulation and Abrupt Climate Change. Annual Review of Marine Science 9, 83–104. https://doi.org/10.1146/annurev-marine-010816-060415

650 Ma, Y., Weldeab, S., Schneider, R.R., Andersen, N., Garbe-Schönberg, D., Friedrich, T., 2021. Strong Southern African Monsoon and weak Mozambique Channel throughflow during Heinrich events: Implication for Agulhas leakage. Earth and Planetary Science Letters 574, 117148. https://doi.org/10.1016/j.epsl.2021.117148

Martrat, B., Grimalt, J.O., Shackleton, N.J., de Abreu, L., Hutterli, M.A., Stocker, T.F., 2007. Four Climate Cycles of Recurring Deep and Surface Water Destabilizations on the Iberian Margin. Science 317, 502–507.
655 https://doi.org/10.1126/science.1139994

McClymont, E.L., Ganeshram, R.S., Pichevin, L.E., Talbot, H.M., van Dongen, B.E., Thunell, R.C., Haywood, A.M., Singarayer, J.S., Valdes, P.J., 2012. Sea-surface temperature records of Termination 1 in the Gulf of California: Challenges for seasonal and interannual analogues of tropical Pacific climate change. Paleoceanography 27. https://doi.org/10.1029/2011PA002226

660 McGee, D., Donohoe, A., Marshall, J., Ferreira, D., 2014. Changes in ITCZ location and cross-equatorial heat transport at the Last Glacial Maximum, Heinrich Stadial 1, and the mid-Holocene. Earth and Planetary Science Letters 390, 69–79. https://doi.org/10.1016/j.epsl.2013.12.043

McManus, J.F., Francois, R., Gherardi, J.-M., Keigwin, L.D., Brown-Leger, S., 2004. Collapse and rapid resumption of Atlantic meridional circulation linked to deglacial climate changes. Nature 428, 834–837. https://doi.org/10.1038/nature02494

Meier, K.J.F., Bahr, A., Chiessi, C.M., Albuquerque, A.L., Raddatz, J., Friedrich, O., 2021. Role of the Tropical Atlantic for the Interhemispheric Heat Transport During the Last Deglaciation. Paleoceanography and Paleoclimatology 36. https://doi.org/10.1029/2020PA004107

Menviel, L.C., Skinner, L.C., Tarasov, L., Tzedakis, P.C., 2020. An ice–climate oscillatory framework for Dansgaard–Oeschger cycles. Nat Rev Earth Environ 1, 677–693. https://doi.org/10.1038/s43017-020-00106-y

Mignac, D., Ferreira, D., Haines, K., 2018. South Atlantic meridional transports from NEMO-based simulations and reanalyses. Ocean Science 14, 53–68. https://doi.org/10.5194/os-14-53-2018

Müller, P.J., Fischer, G., 2004. C37-Alkenones as Paleotemperature Tool: Fundamentals Based on Sediment Traps and Surface Sediments from the South Atlantic Ocean, in: Wefer, G., Mulitza, S., Ratmeyer, V. (Eds.), The South Atlantic in the Late Quaternary: Reconstruction of Material Budgets and Current Systems. Springer, Berlin, Heidelberg, pp. 167–193. https://doi.org/10.1007/978-3-642-18917-3_9

Müller, P.J., Kirst, G., Ruhland, G., von Storch, I., Rosell-Melé, A., 1998. Calibration of the alkenone paleotemperature index U37K′ based on core-tops from the eastern South Atlantic and the global ocean (60°N-60°S). Geochimica et Cosmochimica Acta 62, 1757–1772. https://doi.org/10.1016/S0016-7037(98)00097-0

Nace, T.E., Baker, P.A., Dwyer, G.S., Silva, C.G., Rigsby, C.A., Burns, S.J., Giosan, L., Otto-Bliesner, B., Liu, Z., Zhu, J., 2014. The role of North Brazil Current transport in the paleoclimate of the Brazilian Nordeste margin and paleoceanography of the western tropical Atlantic during the late Quaternary. Palaeogeography, Palaeoclimatology, Palaeoecology 415, 3–13. https://doi.org/10.1016/j.palaeo.2014.05.030

Nascimento, R.A., Santos, T.P., Venancio, I.M., Chiessi, C.M., Ballalai, J.M., Kuhnert, H., Govin, A., Portilho-Ramos, R.C., Lessa, D., Dias, B.B., Pinho, T.M.L., Crivellari, S., Mulitza, S., Albuquerque, A.L.S., 2021a. Origin of δ13C minimum events in thermocline and intermediate waters of the western South Atlantic. Quaternary Science Reviews 272, 107224. https://doi.org/10.1016/j.quascirev.2021.107224

Nascimento, R.A., Venancio, I.M., Chiessi, C.M., Ballalai, J.M., Kuhnert, H., Johnstone, H., Santos, T.P., Prange, M., Govin, A., Crivellari, S., Mulitza, S., Albuquerque, A.L.S., 2021b. Tropical Atlantic stratification response to late Quaternary precessional forcing. Earth and Planetary Science Letters 568, 117030. https://doi.org/10.1016/j.epsl.2021.117030

Nirmal, B., Mohan, K., Tripati, A., Christensen, B.A., Mortyn, P.G., De Vleeschouwer, D., Prakasam, M., Saravanan, K., 2023. Agulhas leakage extension and its influences on South Atlantic surface water hydrography during the Pleistocene. Palaeogeography, Palaeoclimatology, Palaeoecology 615, 111447. https://doi.org/10.1016/j.palaeo.2023.111447

Paillard, D., 1998. The timing of Pleistocene glaciations from a simple multiple-state climate model. Nature 391, 378–381. https://doi.org/10.1038/34891

Pedro, J.B., Jochum, M., Buizert, C., He, F., Barker, S., Rasmussen, S.O., 2018. Beyond the bipolar seesaw: Toward a process understanding of interhemispheric coupling. Quaternary Science Reviews 192, 27–46. https://doi.org/10.1016/j.quascirev.2018.05.005

Peeters, F.J.C., Acheson, R., Brummer, G.-J.A., de Ruijter, W.P.M., Schneider, R.R., Ganssen, G.M., Ufkes, E., Kroon, D., 2004. Vigorous exchange between the Indian and Atlantic oceans at the end of the past five glacial periods. Nature 430, 661–665. https://doi.org/10.1038/nature02785

Piotrowski, A.M., Goldstein, S.L., Hemming, S.R., Fairbanks, R.G., 2005. Temporal Relationships of Carbon Cycling and Ocean Circulation at Glacial Boundaries. Science 307, 1933–1938. https://doi.org/10.1126/science.1104883

Portilho-Ramos, R.C., Chiessi, C.M., Zhang, Y., Mulitza, S., Kucera, M., Siccha, M., Prange, M., Paul, A., 2017. Coupling of equatorial Atlantic surface stratification to glacial shifts in the tropical rainbelt. Scientific Reports 7, 1561. https://doi.org/10.1038/s41598-017-01629-z

Poulton, A.J., Holligan, P.M., Charalampopoulou, A., Adey, T.R., 2017. Coccolithophore ecology in the tropical and subtropical Atlantic Ocean: New perspectives from the Atlantic meridional transect (AMT) programme. Progress in Oceanography, The Atlantic Meridional Transect programme (1995-2016) 158, 150–170. https://doi.org/10.1016/j.pocean.2017.01.003

Prahl, F.G., Wakeham, S.G., 1987. Calibration of unsaturation patterns in long-chain ketone compositions for palaeotemperature assessment. Nature 330, 367–369. https://doi.org/10.1038/330367a0

Rama-Corredor, O., Martrat, B., Grimalt, J.O., López-Otalvaro, G.E., Flores, J.A., Sierro, F., 2015. Parallelisms between sea surface temperature changes in the western tropical Atlantic (Guiana Basin) and high latitude climate signals over the last 140 000 years. Climate of the Past 11, 1297–1311. https://doi.org/10.5194/cp-11-1297-2015

Rasmussen, S.O., Bigler, M., Blockley, S.P., Blunier, T., Buchardt, S.L., Clausen, H.B., Cvijanovic, I., Dahl-Jensen, D., Johnsen, S.J., Fischer, H., Gkinis, V., Guillevic, M., Hoek, W.Z., Lowe, J.J., Pedro, J.B., Popp, T., Seierstad, I.K., Steffensen, J.P., Svensson, A.M., Vallelonga, P., Vinther, B.M., Walker, M.J.C., Wheatley, J.J., Winstrup, M., 2014. A stratigraphic framework for abrupt climatic changes during the Last Glacial period based on three synchronized Greenland ice-core records: refining and extending the INTIMATE event stratigraphy. Quaternary Science Reviews 106, 14–28. https://doi.org/10.1016/j.quascirev.2014.09.007

Reißig, S., Nürnberg, D., Bahr, A., Poggemann, D.-W., Hoffmann, J., 2019. Southward Displacement of the North Atlantic Subtropical Gyre Circulation System During North Atlantic Cold Spells. Paleoceanography and Paleoclimatology 34, 866–885. https://doi.org/10.1029/2018PA003376

Richey, J.N., Hollander, D.J., Flower, B.P., Eglinton, T.I., 2011. Merging late Holocene molecular organic and foraminiferal-based geochemical records of sea surface temperature in the Gulf of Mexico. Paleoceanography 26. https://doi.org/10.1029/2010PA002000

Rodrigues, R.R., Rothstein, L.M., Wimbush, M., 2007. Seasonal Variability of the South Equatorial Current Bifurcation in the Atlantic Ocean: A Numerical Study. Journal of Physical Oceanography 37, 16–30. https://doi.org/10.1175/JPO2983.1

Rodríguez-Zorro, P.A., Ledru, M.-P., Bard, E., Aquino-Alfonso, O., Camejo, A., Daniau, A.-L., Favier, C., Garcia, M., Mineli, T.D., Rostek, F., Ricardi-Branco, F., Sawakuchi, A.O., Simon, Q., Tachikawa, K., Thouveny, N., 2020. Shut down of the South American summer monsoon during the penultimate glacial. Scientific Reports 10, 6275. https://doi.org/10.1038/s41598-020-62888-x

Rühlemann, C., Mulitza, S., Lohmann, G., Paul, A., Prange, M., Wefer, G., 2004. Intermediate depth warming in the tropical Atlantic related to weakened thermohaline circulation: Combining paleoclimate data and modeling results for the last deglaciation. Paleoceanography 19. https://doi.org/10.1029/2003PA000948

Santos, T.P., Ballalai, J.M., Franco, D.R., Oliveira, R.R., Lessa, D.O., Venancio, I.M., Chiessi, C.M., Kuhnert, H., Johnstone, H., Albuquerque, A.L.S., 2020. Asymmetric response of the subtropical western South Atlantic thermocline to the Dansgaard-Oeschger events of Marine Isotope Stages 5 and 3. Quaternary Science Reviews 237, 106307. https://doi.org/10.1016/j.quascirev.2020.106307

Santos, T.P., Belem, A.L., Barbosa, C.F., Dokken, T., Albuquerque, A.L.S., 2014. Paleoceanographic reconstruction of the western equatorial Atlantic during the last 40 kyr. Palaeogeography, Palaeoclimatology, Palaeoecology 415, 14–20. https://doi.org/10.1016/j.palaeo.2014.01.001

Santos, T.P., Lessa, D.O., Venancio, I.M., Chiessi, C.M., Mulitza, S., Kuhnert, H., Govin, A., Machado, T., Costa, K.B., Toledo, F., Dias, B.B., Albuquerque, A.L.S., 2017. Prolonged warming of the Brazil Current precedes deglaciations. Earth and Planetary Science Letters 463, 1–12. https://doi.org/10.1016/j.epsl.2017.01.014

Santos, T.P., Shimizu, M.H., Nascimento, R.A., Venancio, I.M., Campos, M.C., Portilho-Ramos, R.C., Ballalai, J.M., Lessa, D.O., Crivellari, S., Nagai, R.H., Chiessi, C.M., Kuhnert, H., Bahr, A., Albuquerque, A.L.S., 2022. A data-model perspective on the Brazilian margin surface warming from the Last Glacial Maximum to the Holocene. Quaternary Science Reviews 286, 107557. https://doi.org/10.1016/j.quascirev.2022.107557

Schettini, C.A.F., Domingues, E. de C., Truccolo, E.C., Oliveira Filho, J.C. de, Mazzini, P.L.F., 2017. Seasonal variability of water masses and currents at the eastern Brazilian continental shelf (7.5–9 ∘ S). Regional Studies in Marine Science 16, 131–144. https://doi.org/10.1016/j.rsma.2017.08.012

Schlitzer, R., 2020. Ocean Data View.

Schmidt, M.W., Chang, P., Hertzberg, J.E., Them, T.R., Ji, L., Otto-Bliesner, B.L., 2012. Impact of abrupt deglacial climate change on tropical Atlantic subsurface temperatures. Proceedings of the National Academy of Sciences 109, 14348–14352. https://doi.org/10.1073/pnas.1207806109

Schott, F.A., Fischer, J., Stramma, L., 1998. Transports and Pathways of the Upper-Layer Circulation in the Western Tropical Atlantic. J. Phys. Oceanogr. 28, 1904–1928. https://doi.org/10.1175/1520-0485(1998)028<1904:TAPOTU>2.0.CO;2

Schott, F.A., Stramma, L., Fischer, J., 1995. The warm water inflow into the western tropical Atlantic boundary regime, spring 1994. J. Geophys. Res. 100, 24745. https://doi.org/10.1029/95JC02803

Schouten, S., Hopmans, E.C., Schefuß, E., Sinninghe Damsté, J.S., 2002. Distributional variations in marine crenarchaeotal membrane lipids: a new tool for reconstructing ancient sea water temperatures? Earth and Planetary Science Letters 204, 265–274. https://doi.org/10.1016/S0012-821X(02)00979-2

Schouten, S., Hopmans, E.C., Sinninghe Damsté, J.S., 2013. The organic geochemistry of glycerol dialkyl glycerol tetraether lipids: A review. Organic Geochemistry 54, 19–61. https://doi.org/10.1016/j.orggeochem.2012.09.006

Scussolini, P., Marino, G., Brummer, G.-J.A., Peeters, F.J.C., 2015. Saline Indian Ocean waters invaded the South Atlantic thermocline during glacial termination II. Geology 43, 139–142. https://doi.org/10.1130/G36238.1

Sikes, E.L., Farrington, J.W., Keigwin, L.D., 1991. Use of the alkenone unsaturation ratio U37k to determine past sea surface temperatures: core-top SST calibrations and methodology considerations. Earth and Planetary Science Letters 104, 36–47. https://doi.org/10.1016/0012-821X(91)90235-A

Simon, M.H., Ziegler, M., Bosmans, J., Barker, S., Reason, C.J.C., Hall, I.R., 2015. Eastern South African hydroclimate over the past 270,000 years. Scientific Reports 5, 18153. https://doi.org/10.1038/srep18153

Smith, J.M., Chavez, F.P., Francis, C.A., 2014. Ammonium Uptake by Phytoplankton Regulates Nitrification in the Sunlit Ocean. PLOS ONE 9, e108173. https://doi.org/10.1371/journal.pone.0108173

Souza, A.G.Q. de, Kerr, R., Azevedo, J.L.L. de, 2018. On the influence of Subtropical Mode Water on the South Atlantic Ocean. Journal of Marine Systems 185, 13–24. https://doi.org/10.1016/j.jmarsys.2018.04.006

Stocker, T.F., 2000. Past and future reorganizations in the climate system. Quaternary Science Reviews 19, 301–319. https://doi.org/10.1016/S0277-3791(99)00067-0

Stocker, T.F., Johnsen, S.J., 2003. A minimum thermodynamic model for the bipolar seesaw. Paleoceanography 18. https://doi.org/10.1029/2003PA000920

Stramma, L., England, M., 1999. On the water masses and mean circulation of the South Atlantic Ocean. Journal of Geophysical Research: Oceans 104, 20863–20883. https://doi.org/10.1029/1999JC900139

Sun, S., Thompson, A.F., Xie, S.-P., Long, S.-M., 2022. Indo-Pacific Warming Induced by a Weakening of the Atlantic Meridional Overturning Circulation. Journal of Climate 35, 815–832.

Tierney, J.E., Tingley, M.P., 2018. BAYSPLINE: A New Calibration for the Alkenone Paleothermometer. Paleoceanography and Paleoclimatology 33, 281–301. https://doi.org/10.1002/2017PA003201

Tierney, J.E., Tingley, M.P., 2015. A TEX86 surface sediment database and extended Bayesian calibration. Scientific Data 2, 150029. https://doi.org/10.1038/sdata.2015.29

Tierney, J.E., Tingley, M.P., 2014. A Bayesian, spatially-varying calibration model for the TEX86 proxy. Geochimica et Cosmochimica Acta 127, 83–106. https://doi.org/10.1016/j.gca.2013.11.026

Trenberth, K.E., Fasullo, J.T., 2017. Atlantic meridional heat transports computed from balancing Earth's energy locally. Geophysical Research Letters 44, 1919–1927. https://doi.org/10.1002/2016GL072475

Venancio, I.M., Mulitza, S., Govin, A., Santos, T.P., Lessa, D.O., Albuquerque, A.L.S., Chiessi, C.M., Tiedemann, R., Vahlenkamp, M., Bickert, T., Schulz, M., 2018. Millennial- to Orbital-Scale Responses of Western Equatorial Atlantic Thermocline Depth to Changes in the Trade Wind System Since the Last Interglacial. Paleoceanography and Paleoclimatology 33, 1490–1507. https://doi.org/10.1029/2018PA003437

Vink, A., Rühlemann, C., Zonneveld, K.A.F., Mulitza, S., Hüls, M., Willems, H., 2001. Shifts in the position of the north equatorial current and rapid productivity changes in the western tropical Atlantic during the last glacial. Paleoceanography 16, 479–490. https://doi.org/10.1029/2000PA000582

Waelbroeck, C., Pichat, S., Böhm, E., Lougheed, B.C., Faranda, D., Vrac, M., Missiaen, L., Vazquez Riveiros, N., Burckel, P., Lippold, J., Arz, H.W., Dokken, T., Thil, F., Dapoigny, A., 2018. Relative timing of precipitation and ocean circulation changes in the western equatorial Atlantic over the last 45 kyr. Climate of the Past 14, 1315–1330. https://doi.org/10.5194/cp-14-1315-2018

Wang, X., Auler, A.S., Edwards, R.L., Cheng, H., Cristalli, P.S., Smart, P.L., Richards, D.A., Shen, C.-C., 2004. Wet periods in northeastern Brazil over the past 210 kyr linked to distant climate anomalies. Nature 432, 740–743. https://doi.org/10.1038/nature03067

Wang, Y., Olascoaga, M.J., Beron-Vera, F.J., 2015. Coherent water transport across the South Atlantic. Geophysical Research Letters 42, 4072–4079. https://doi.org/10.1002/2015GL064089

Weijers, J.W.H., Schefuß, E., Kim, J.-H., Sinninghe Damsté, J.S., Schouten, S., 2014. Constraints on the sources of branched tetraether membrane lipids in distal marine sediments. Organic Geochemistry 72, 14–22. https://doi.org/10.1016/j.orggeochem.2014.04.011

Weldeab, S., Schneider, R.R., Kölling, M., 2006. Deglacial sea surface temperature and salinity increase in the western tropical Atlantic in synchrony with high latitude climate instabilities. Earth and Planetary Science Letters 241, 699–706. https://doi.org/10.1016/j.epsl.2005.11.012

Wilson, K.E., Maslin, M.A., Burns, S.J., 2011. Evidence for a prolonged retroflection of the North Brazil Current during glacial stages. Palaeogeography, Palaeoclimatology, Palaeoecology 301, 86–96. https://doi.org/10.1016/j.palaeo.2011.01.003

Wu, L., Li, C., Yang, C., Xie, S.-P., 2008. Global Teleconnections in Response to a Shutdown of the Atlantic Meridional Overturning Circulation*. Journal of Climate 21, 3002–3019. https://doi.org/10.1175/2007JCLI1858.1

Xie, S.-P., Tanimoto, Y., Noguchi, H., Matsuno, T., 1999. How and why climate variability differs between the tropical Atlantic and Pacific. Geophysical Research Letters 26, 1609–1612. https://doi.org/10.1029/1999GL900308

Zakem, E.J., Al-Haj, A., Church, M.J., van Dijken, G.L., Dutkiewicz, S., Foster, S.Q., Fulweiler, R.W., Mills, M.M., Follows, M.J., 2018. Ecological control of nitrite in the upper ocean. Nature Communications 9, 1206. https://doi.org/10.1038/s41467-018-03553-w

Zhang, Y.G., Liu, X., 2018. Export Depth of the TEX86 Signal. Paleoceanography and Paleoclimatology 33, 666–671. https://doi.org/10.1029/2018PA003337

Zhang, Y.G., Pagani, M., Wang, Z., 2016. Ring Index: A new strategy to evaluate the integrity of TEX $_{86}$ paleothermometry. Paleoceanography 31, 220–232. https://doi.org/10.1002/2015PA002848

Zhang, Y.G., Zhang, C.L., Liu, X.-L., Li, L., Hinrichs, K.-U., Noakes, J.E., 2011. Methane Index: A tetraether archaeal lipid biomarker indicator for detecting the instability of marine gas hydrates. Earth and Planetary Science Letters 307, 525–534. https://doi.org/10.1016/j.epsl.2011.05.031

Captions of Figures and Tables

Figure 1: Regional oceanographic settings. Left panel: Upper South Atlantic Ocean currents and investigated (previously published) sediments cores plotted on the mean annual sea temperature at 150 m depth (World Ocean Atlas 2013) plotted at 1°x1° grid and spatially interpolated using DIVA gridding (Ocean Data View software, Schlitzer, 2005). AC = Agulhas Current, AL = Agulhas Leakage, SEC = South Equatorial Current, SECC = South Equatorial Counter Current, NECC = North Equatorial Counter Current, NEC = North Equatorial Current, NBUC = North Brazil Undercurrent, NBC = North Brazil Current, BC = Brazil Current, MC = Malvinas Current, SAC = South Atlantic Current. GL-1180 (this study), MD96-2048 (Caley et al., 2011), MD96-2080 and MD02-2594 (Kasper et al., 2014), CBR (Peeters et al., 2004), 64PE-174P13 (Scussolini et al., 2015), GL-1090 (Santos et al., 2017), GeoB3910-2 (Waelbroeck et al., 2018), GL-1248 (Venancio et al., 2018), VM12-107 (Schmidt et al., 2012), SO164-03-4 (Reißig et al., 2019), GeoB9528-3 (Lopes dos Santos et al., 2010). Right panel: Annual and seasonal temperature profiles at 8.5°S, 33.5°W (World Ocean Atlas 13).

Figure 2: Molecular structure of long-chain C_{37} alkenones and isoprenoid GDGTs for the calculation of temperature proxies

Figure 3: New temperature records (this study) compared to previously published records in the GL-1180 core: A) $U^{K'}_{37}$-derived sea surface temperature ($U^{K'}_{37}$-SST) using the global calibration at 0 m (Müller et al., 1998) record of GL-1180 core, this study; B) TEX^{H}_{86}-derived upper thermocline temperature (TEX^{H}_{86}-SubT) TEX_{86} calculated with the equation from Schouten et al., (2002) and inferred upper thermocline temperature (Kim et al., 2010) record of GL-1180 core, this study; C) Mg/Ca-main thermocline temperature (Mg/Ca-ThT) based on *G. truncatulinoides*, GL-1180 core (Nascimento et al., 2021b), thick black line representing 3-points running-average. The y-scale is reduced twice compared to organic proxies; D) benthic foraminifera $\delta^{13}C$ (*Cibicides spp.*), GL-1180 core (Nascimento et al., 2021b); E) benthic foraminifera $\delta^{18}O$ (*Cibicides spp.*) in black, GL-1180 core (Nascimento et al., 2021a), thick black line representing 3-points running-average. Dark and light shaded areas represent interglacial periods and glacial terminations (TI, TII and TIII) respectively. Squared numbers refers to Marine Isotope Stages (MIS 1 to MIS 9) identified on the benthic foraminifera $\delta^{18}O$ record of GL-1180. Total mean (calibration + analytical) errors are represented along the Y-axes for $U^{K'}_{37}$-SST and TEX^{H}_{86}-SubT.

Figure 4: Western South Atlantic records of sea temperature -ST- (SST for surface, SubT for upper thermocline, ThT for main thermocline) over the last 3 glacial terminations, on their respective original chronologies. A) SST (TEX^{H}_{86}) and SubT ($U^{K'}_{37}$) temperature records of GL-1090 core (Cruz et al., 2023). B) SST (Mg/Ca, *G. ruber*) and ThT (Mg/Ca *G. inflata*) temperature records of GL-1090 core

(Ballalai et al., 2019; Santos et al., 2017). C) SST stack (presented in temperature anomaly versus the late Holocene) for the Brazilian margin (17 records) (Santos et al., 2022). D) SST ($U^{K'}_{37}$) and SubT (TEX^{H}_{86}) temperature records of GL-1180 core, this study. E) Benthic foraminifera $\delta^{18}O$ records for the above-mentioned cores. Light shaded areas represent glacial terminations (identified on respective benthic foraminifera $\delta^{18}O$ records). Dark shaded areas represent the Heinrich Event 1 (H1) and the Younger Dryas (YD). The Bølling-Allerød (B/A) event is also indicated.

Figure 5: Investigating the Bipolar Seesaw impacts in the equatorial and subtropical western South Atlantic for the last 110 kyr. Above dash lines, selected paleoclimate records illustrating regional oceanic response to last glacial AMOC changes: A) Ice $\delta^{18}O$ of NGRIP Greenland Ice core project (NorthGRIP Comm. Members, 2004); B) C_{37} alkenone derived-sea surface temperature ($U^{K'}_{37}$-SST) of GeoB3910-2 (Jaeschke et al., 2007); C) benthic foraminifera (*C. wuellerstorfi*) $\delta^{13}C$ of core GeoB3910-2 (Waelbroeck et al., 2018). Below dash lines, selected records showing thermocline changes on the Brazilian margins: D) upper ocean stratification $\Delta\delta^{18}O$ (between *G. ruber* and *N. dutertrei*) in core GL-1248 (Venancio et al., 2018); E) upper thermocline temperature (TEX^{H}_{86}-SubT) of GL-1180 record (this study); F) thermocline dwelling *Globorotalia inflata* Mg/Ca-derived main thermocline temperature (Mg/Ca-ThT) from GL-1090 record (Santos et al., 2020); G) $\delta^{18}O$ sea-water corrected for ice-volume changes and Mg/Ca-derived main thermocline temperature (*G. truncatulinoides*, Mg/Ca-ThT) of core GL-1180 (Nascimento et al., 2021b).

Figure 6: Records of the Agulhas Leakage. A) Difference between $U^{K'}_{37}$ and TEX^{H}_{86} temperatures (ΔST) in the MD96-2048 record (Caley et al., 2011); B) SST records of the MD96-2048 (Caley et al., 2011); C) Difference between $U^{K'}_{37}$-SST and TEX^{H}_{86}-SubT temperature (ΔST) in the GL-1180 core (this study); D) $U^{K'}_{37}$-SST record in CBR (*Cape Basin Records*) cores (Peeters et al., 2004); E) Agulhas Leakage fauna assemblages in the CBR cores (Peeters et al., 2004); F) benthic foraminifera $\delta^{18}O$ records of cores MD96-2048 (Caley et al., 2011), CBR (Peeters et al., 2004) and GL-1180 (this study).

Figure 7: Sea Temperature (ST) records exhibiting a strong subsurface warming over deglacial interval from the Indian Ocean to the western tropical North Atlantic. A) SST (Mg/Ca, *G. ruber*) and main thermocline seawater temperature (Mg/Ca-ThT, *G. truncatulinoides*) records of core SO164-03-4 (Reißig et al., 2019). B) SST ($U^{K'}_{37}$) and SubT (TEX^{H}_{86}) temperature records of GeoB9528-3 core (Lopes dos Santos et al., 2010). C) SST ($U^{K'}_{37}$) and SubT (TEX^{H}_{86}) temperature records of MD96-2080 (Termination I) and MD02-2594 (TII) core (Kasper et al., 2014). D) SST ($U^{K'}_{37}$) and SubT (TEX^{H}_{86}) temperature records of GL-1180 core (this study). E) SST ($U^{K'}_{37}$) and SubT (TEX^{H}_{86}) temperature records of MD96-2048 core (Caley et al., 2011). F) Benthic foraminifera $\delta^{18}O$ records for the above-mentioned cores for which data are available. Dark shaded areas represent deglacial intervals (noted TI, TII and TIII) and blue

shaded areas represent the Heinrich Event 1 (H1) and the Younger Dryas (YD). The Bølling-Allerød (B/A) event is also indicated.
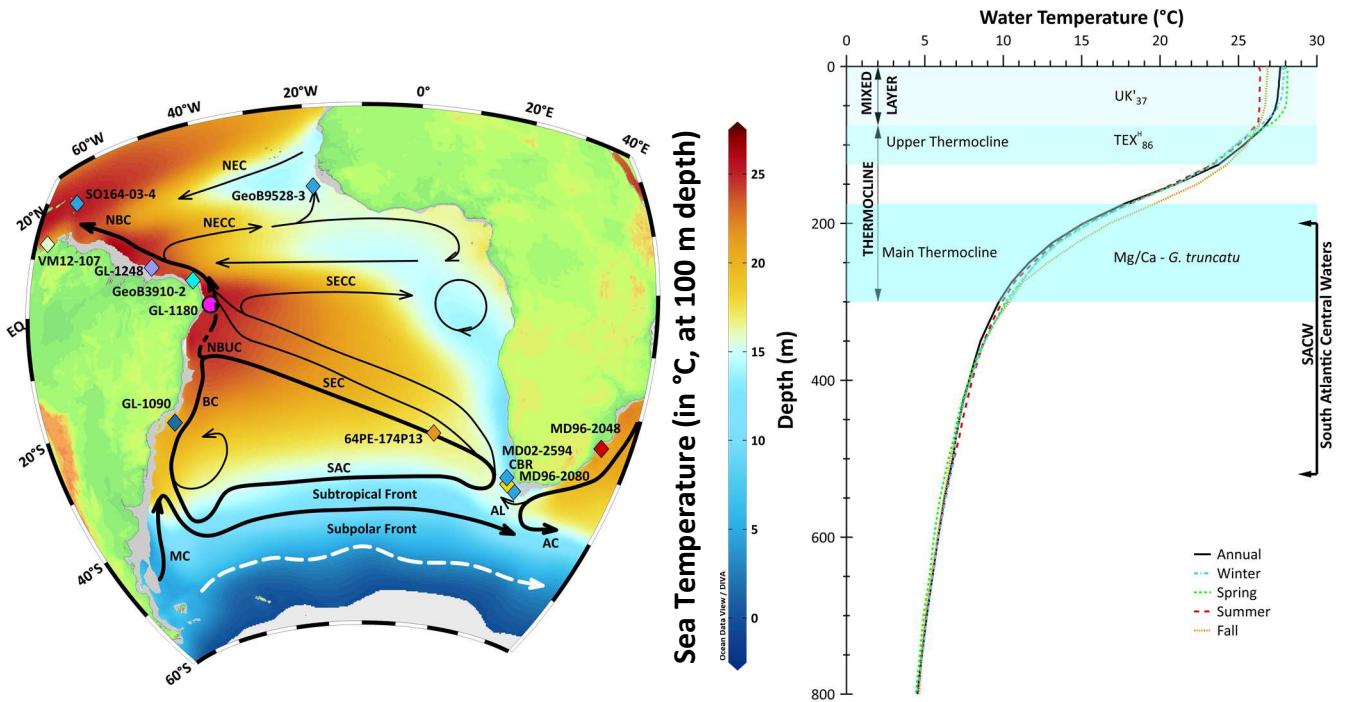
Figure 8: Schematic view of upper ocean temperature and surface currents during classical fullglacial interval (left) and the later deglacial period (right). Position of core exhibiting a surface and subsurface warmings over at least, one glacial termination are shown: VM12-107 (VM12 on the map, Schmidt et al., 2012), M78/1-235-1 (M78/1 on the map, Reißig et al., 2019), GeoB9528-3 (Lopes dos Santos et al., 2010), GL-1180 (*this study*), GL-1090 (Santos et al., 2017), 64Pe-174P13 (64PE on the map, Scussolini et al., 2015), MD02-2594 (2594 on the map, Kasper et al., 2014), MD96-2080 (2082 on the map, Kasper et al., 2014) and MD96-2048 (2048 on the map, Caley et al., 2011) cores used to explain the temperature pattern and circulations changes. Dotted lines correspond to winds (North-East trades and mid-latitudes westerlies). Solid arrows (thick when the current is strong, thin when it is weak) correspond to surface current: Agulhas Current (AC), Agulhas Leakage (AL), South-Equatorial Current (SEC), Brazil Current (BC), South Atlantic Current (SAC), North Brazil Current (NBC), North Equatorial Counter Current (NECC) and North Equatorial Current (NEC). Colour represent roughly upper ocean temperature between hot (red), temperate (orange) and cold (blue).
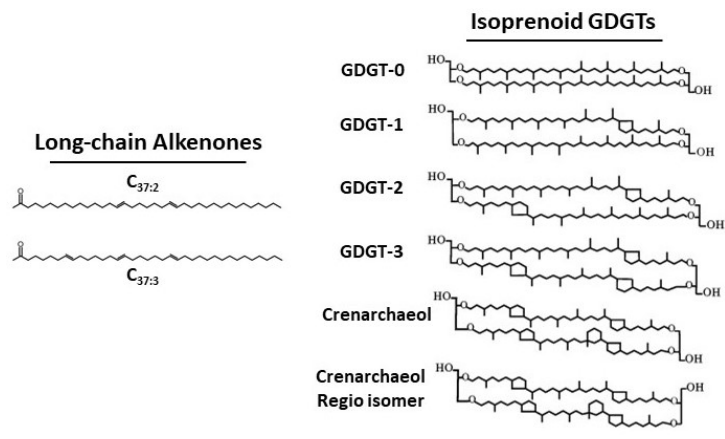
Figures

Figure 9: Regional oceanographic settings. Left panel: Upper South Atlantic Ocean currents and investigated (previously published) sediments cores plotted on the mean annual sea temperature at 150 m depth (World Ocean Atlas 2013) plotted at 1°x1° grid and spatially interpolated using DIVA gridding (Ocean Data View software, Schlitzer, 2005). AC = Agulhas Current, AL = Agulhas Leakage, SEC = South Equatorial Current, SECC = South Equatorial Counter Current, NECC = North Equatorial Counter Current, NEC = North Equatorial Current, NBUC = North Brazil Undercurrent, NBC = North Brazil Current, BC = Brazil Current, MC = Malvinas Current, SAC = South Atlantic Current. GL-1180 (this study), MD96-2048 (Caley et al., 2011), MD96-2080 and MD02-2594 (Kasper et al., 2014), CBR (Peeters et al., 2004), 64PE-174P13 (Scussolini et al., 2015), GL-1090 (Santos et al., 2017), GeoB3910-2 (Waelbroeck et al., 2018), GL-1248 (Venancio et al., 2018), VM12-107 (Schmidt et al., 2012), SO164-03-4 (Reißig et al., 2019), GeoB9528-3 (Lopes dos Santos et al., 2010). Right panel: Annual and seasonal temperature profiles at 8.5°S, 33.5°W (World Ocean Atlas 13).

4

Figure 10: Molecular structure of long-chain C$_{37}$ alkenones and isoprenoid GDGTs for the calculation of temperature proxies

105

5

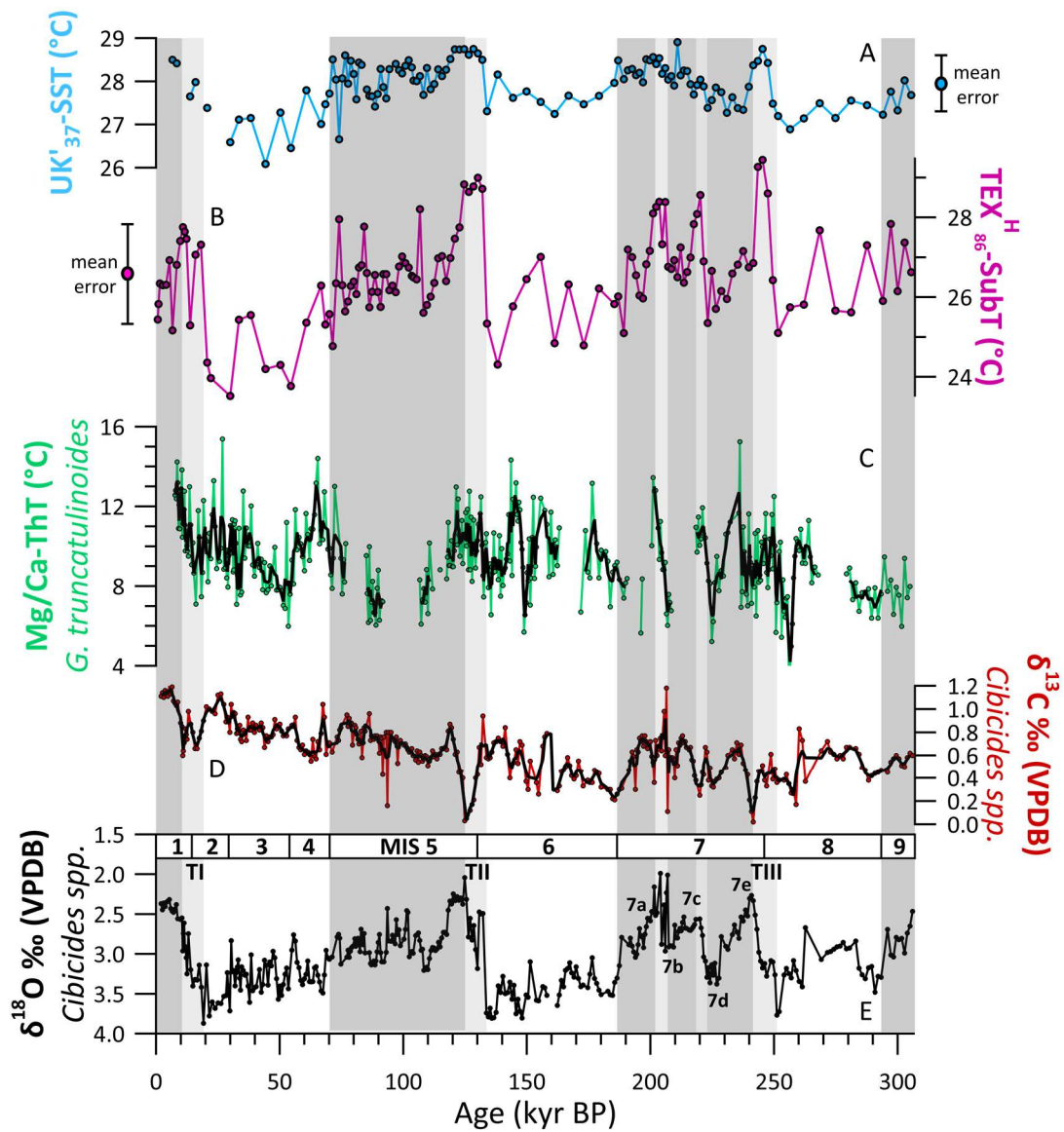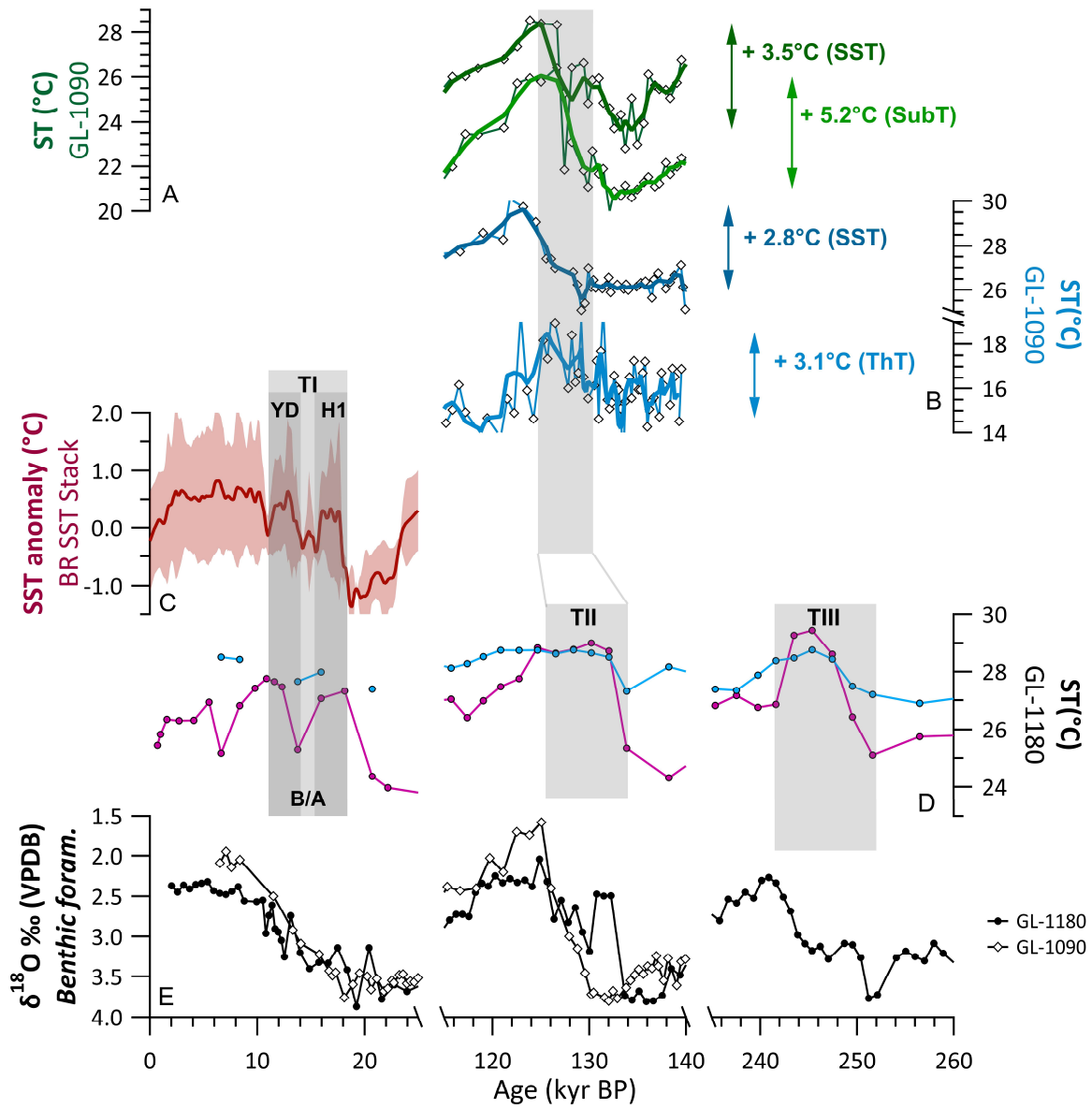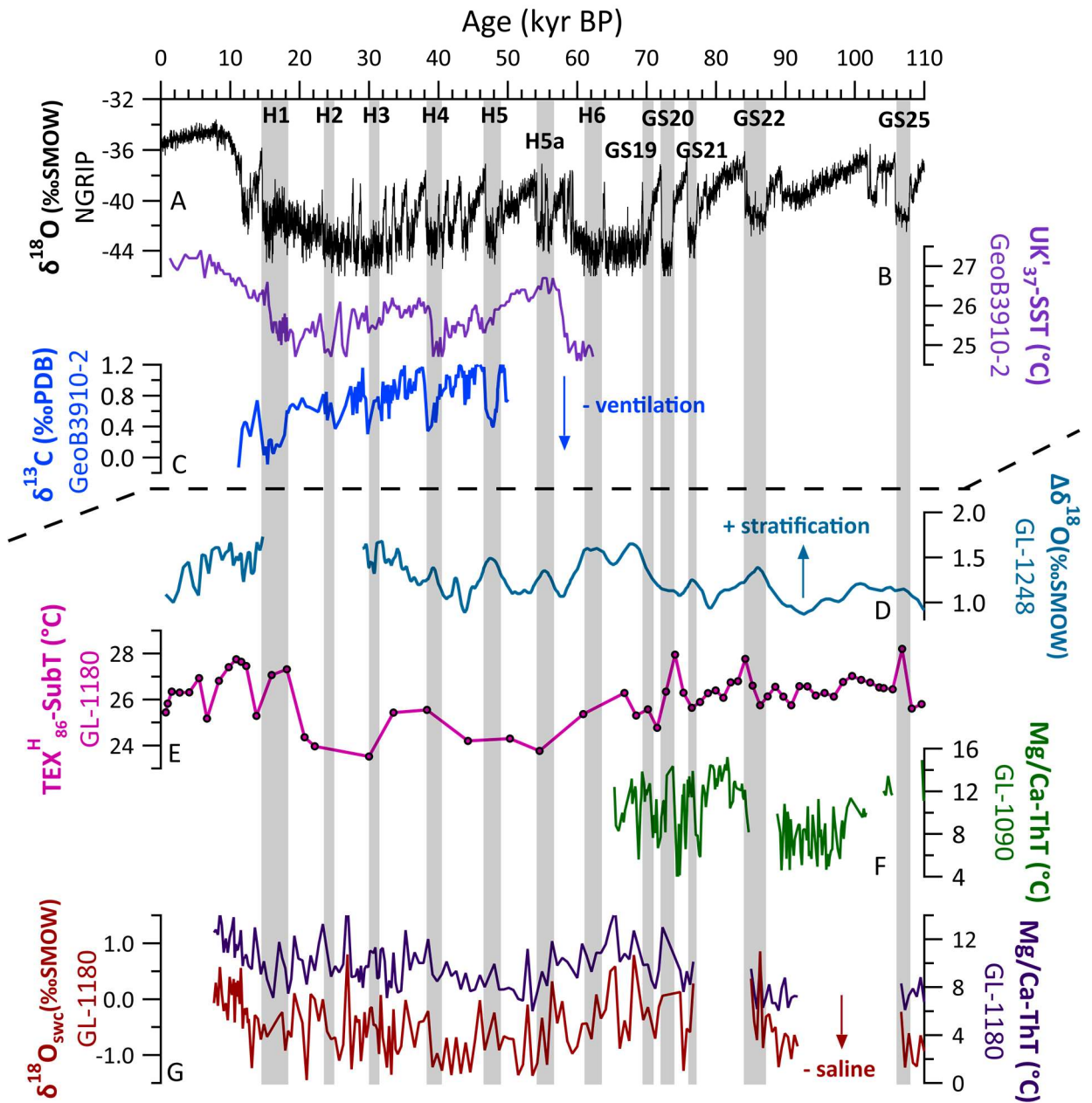**Figure 11: New temperature records (this study) compared to previously published records in the GL-1180 core: A) $U^{K'}_{37}$-derived sea surface temperature ($U^{K'}_{37}$-SST) using the global calibration at 0 m (Müller et al., 1998) record of GL-1180 core, this study; B) TEX^H_{86}-derived upper thermocline temperature (TEX^H_{86}-SubT) TEX_{86} calculated with the equation from Schouten et al., (2002) and inferred upper thermocline temperature (Kim et al., 2010) record of GL-1180 core, this study; C) Mg/Ca-main thermocline temperature (Mg/Ca-ThT) based on *G. truncatulinoides*, GL-1180 core (Nascimento et al., 2021b), thick black line representing 3-points running-average. The y-scale is reduced twice compared to organic proxies; D) benthic foraminifera δ^{13}C (*Cibicides spp.*), GL-1180 core (Nascimento et al., 2021b); E) benthic foraminifera δ^{18}O (*Cibicides spp.*) in black, GL-1180 core (Nascimento et al., 2021a), thick black line representing 3-points running-average. Dark and light shaded areas represent interglacial periods and glacial terminations (TI, TII and TIII) respectively. Squared numbers refers to Marine Isotope Stages (MIS 1 to MIS 9) identified on the benthic foraminifera δ^{18}O record of GL-1180. Total mean (calibration + analytical) errors are represented along the Y-axes for $U^{K'}_{37}$-SST and TEX^H_{86}-SubT.**

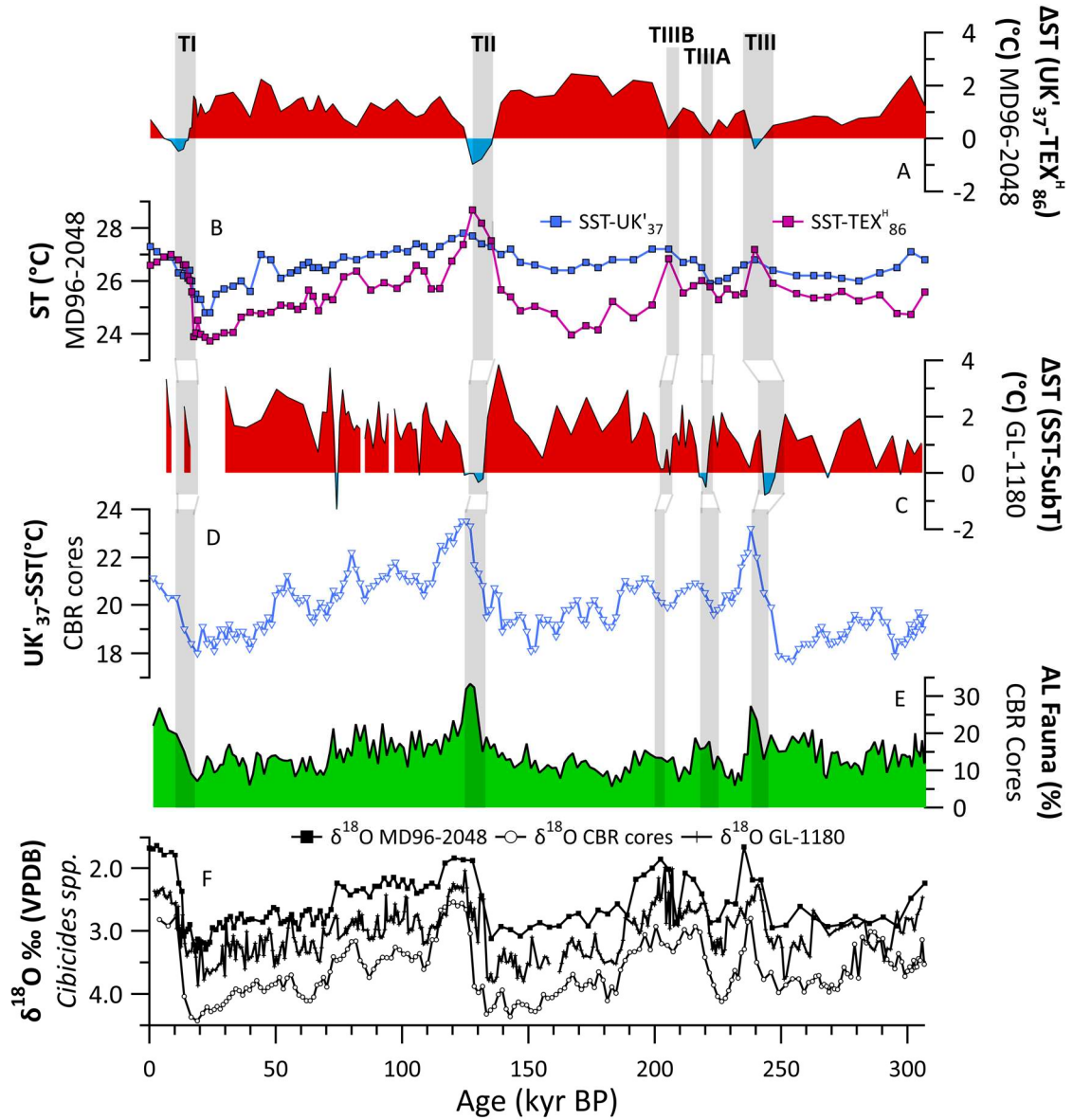**Figure 12: Western South Atlantic records of sea temperature -ST- (SST for surface, SubT for upper thermocline, ThT for main thermocline) over the last 3 glacial terminations, on their respective original chronologies. A)** SST (TEX$^H_{86}$) and SubT (U$^{K'}_{37}$) temperature records of GL-1090 core (Cruz et al., 2023). **B)** SST (Mg/Ca, *G. ruber*) and ThT (Mg/Ca *G. inflata*) temperature records of GL-1090 core (Ballalai et al., 2019; Santos et al., 2017). **C)** SST stack (presented in temperature anomaly versus the late Holocene) for the Brazilian margin (17 records) (Santos et al., 2022). **D)** SST (U$^{K'}_{37}$) and SubT (TEX$^H_{86}$) temperature records of GL-1180 core, this study. **E)** Benthic foraminifera δ^{18}O records for the above-mentioned cores. Light shaded areas represent glacial terminations (identified on respective benthic foraminifera δ^{18}O records). Dark shaded areas represent the Heinrich Event 1 (H1) and the Younger Dryas (YD). The Bølling-Allerød (B/A) event is also indicated.
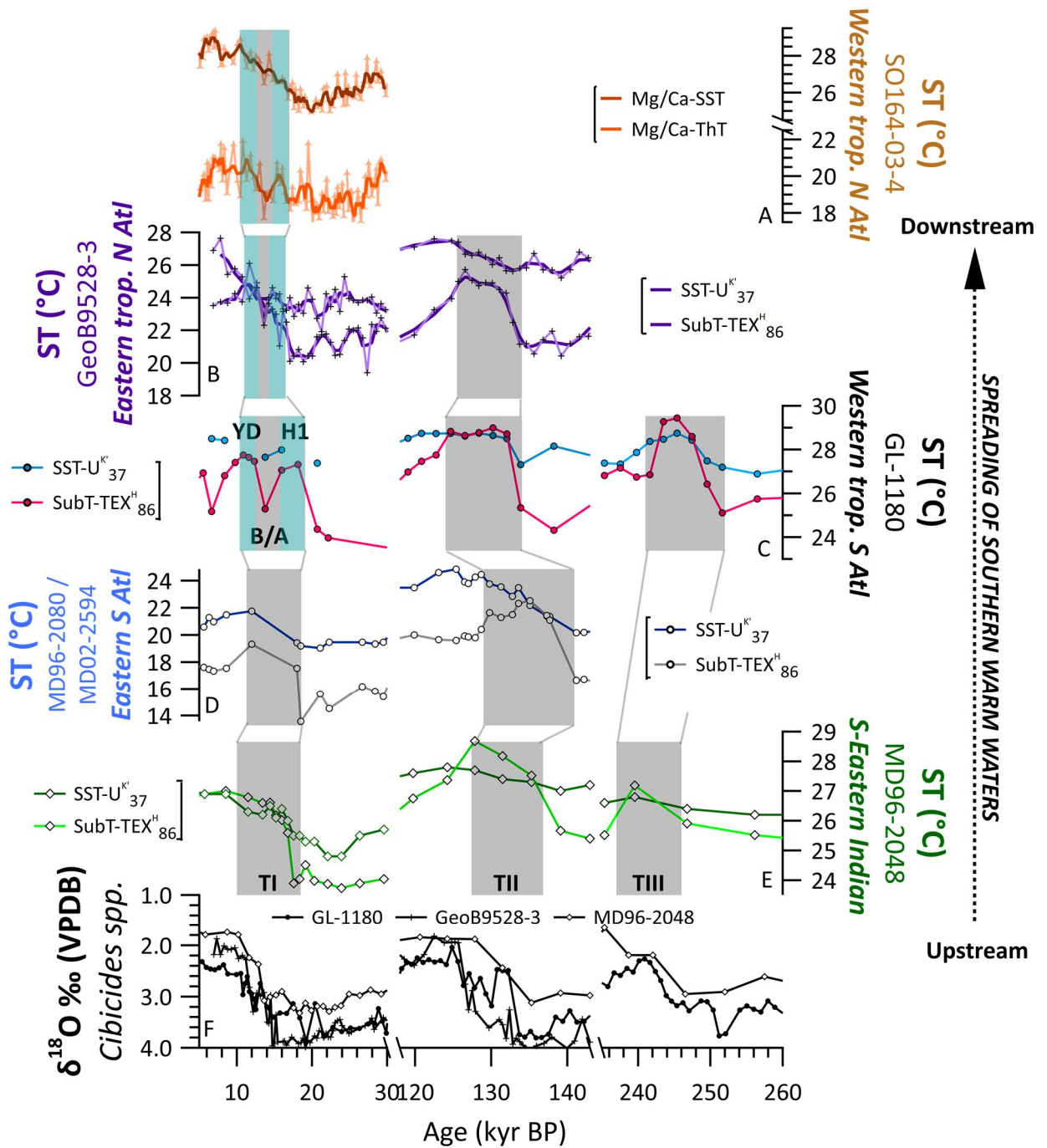
7

Figure 13: Investigating the Bipolar Seesaw impacts in the equatorial and subtropical western South Atlantic for the last 110 kyr. Above dash lines, selected paleoclimate records illustrating regional oceanic response to last glacial AMOC changes: A) Ice $\delta^{18}O$ of NGRIP Greenland Ice core project (NorthGRIP Comm. Members, 2004); B) C_{37} alkenone derived-sea surface temperature ($U^{K'}_{37}$-SST) of GeoB3910-2 (Jaeschke et al., 2007); C) benthic foraminifera (*C. wuellerstorfi*) $\delta^{13}C$ of core GeoB3910-2 (Waelbroeck et al., 2018). Below dash lines, selected records showing thermocline changes on the Brazilian margins: D) upper ocean stratification $\Delta\delta^{18}O$ (between *G. ruber* and *N. dutertrei*) in core GL-1248 (Venancio et al., 2018); E) upper thermocline temperature (TEX^{H}_{86}-SubT) of GL-1180 record (this study); F) thermocline dwelling *Globorotalia inflata* Mg/Ca-derived main thermocline temperature (Mg/Ca-

8

140 **Figure 14: Records of the Agulhas Leakage. A)** Difference between $U^{K'}_{37}$ and TEX^{H}_{86} temperatures (ΔST) in the MD96-2048 record (Caley et al., 2011); **B)** SST records of the MD96-2048 (Caley et al., 2011); **C)** Difference between $U^{K'}_{37}$-SST and TEX^{H}_{86}-SubT temperature (ΔST) in the GL-1180 core (this study); **D)** $U^{K'}_{37}$-SST record in CBR (*Cape Basin Records*) cores (Peeters et al., 2004); **E)** Agulhas Leakage fauna assemblages in the CBR cores (Peeters et al., 2004); **F)** benthic foraminifera δ18O records of cores MD96-2048 (Caley et al., 2011), CBR (Peeters et al., 2004) and GL-1180 (this study).

9

Figure 15: Sea Temperature (ST) records exhibiting a strong subsurface warming over deglacial interval from the Indian Ocean to the western tropical North Atlantic. A) SST (Mg/Ca, *G. ruber*) and main thermocline seawater temperature (Mg/Ca-ThT, *G. truncatulinoides*) records of core SO164-03-4 (Reißig et al., 2019). B) SST (U$^{K'}_{37}$) and SubT (TEX$^H_{86}$) temperature records of GeoB9528-3 core (Lopes dos Santos et al., 2010). C) SST (U$^{K'}_{37}$) and SubT (TEX$^H_{86}$) temperature records of MD96-2080 (Termination I) and MD02-2594 (TII) core (Kasper et al., 2014). D) SST (U$^{K'}_{37}$) and SubT (TEX$^H_{86}$) temperature records of GL-

145

10

1180 core (this study). E) SST ($U^{K'}_{37}$) and SubT (TEX^H_{86}) temperature records of MD96-2048 core (Caley et al., 2011). F) Benthic foraminifera $\delta^{18}O$ records for the above-mentioned cores for which data are available. Dark shaded areas represent deglacial intervals (noted TI, TII and TIII) and blue shaded areas represent the Heinrich Event 1 (H1) and the Younger Dryas (YD). The Bølling-Allerød (B/A) event is also indicated.
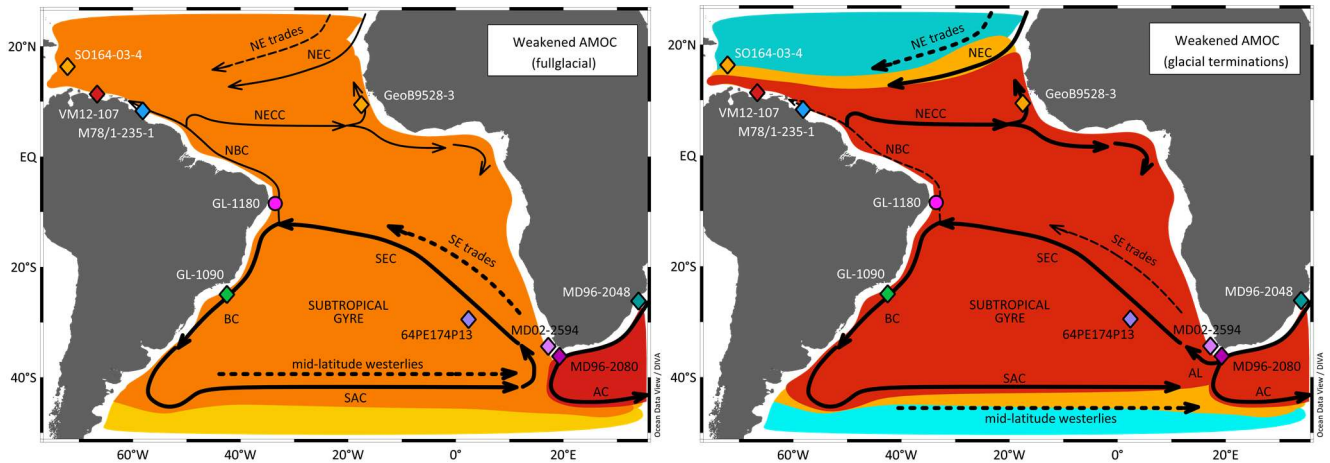
155

Figure 16: Schematic view of upper ocean temperature and surface currents during classical fullglacial interval (left) and the later deglacial period (right). Position of core exhibiting a surface and subsurface warmings over at least, one glacial termination are shown: VM12-107 (VM12 on the map, Schmidt et al., 2012), M78/1-235-1 (M78/1 on the map, Reißig et al., 2019), GeoB9528-3 (Lopes dos Santos et al., 2010), GL-1180 (*this study*), GL-1090 (Santos et al., 2017), 64Pe-174P13 (64PE on the map, Scussolini et al., 2015), MD02-2594 (2594 on the map, Kasper et al., 2014), MD96-2080 (2082 on the map, Kasper et al., 2014) and MD96-2048 (2048 on the map, Caley et al., 2011) cores used to explain the temperature pattern and circulations changes. Dotted lines correspond to winds (North-East trades and mid-latitudes westerlies). Solid arrows (thick when the current is strong, thin when it is weak) correspond to surface current: Agulhas Current (AC), Agulhas Leakage (AL), South-Equatorial Current (SEC), Brazil Current (BC), South Atlantic Current (SAC), North Brazil Current (NBC), North Equatorial Counter Current (NECC) and North Equatorial Current (NEC). Colour represent roughly upper ocean temperature between hot (red), temperate (orange) and cold (blue).